CHAPTER 9

Simulations of Morphology and Charge Transport in Supramolecular Organic Materials

DENIS ANDRIENKO

Max Planck Institute for Polymer Research, Ackermannweg 10,
55128 Mainz, Germany
Email: denis.andrienko@mpip-mainz.mpg.de

9.1 Introduction

Conjugated polymers and cyclic π-systems have been studied for almost a decade in order to develop various optoelectronic devices, such as light-emitting diodes, field effect transistors, optically pumped lasers, and organic solar cells. Progress in the field has been remarkable, with the recently announced 12% efficient organic solar cells and light emitting diodes (OLEDs), having already entered the market of flat panel displays and lighting applications. Despite these advancements, there is still a lack of understanding of the fundamental processes taking place in the active layers of such devices, hindering further development. This is, however, hardly surprising considering the complexity of the processes involved, where one needs to have a thorough understanding of a system's behavior on multiple time- and length-scales.

RSC Smart Materials No. 12
Supramolecular Materials for Opto-Electronics
Edited by Norbert Koch

Published by the Royal Society of Chemistry, www.rsc.org

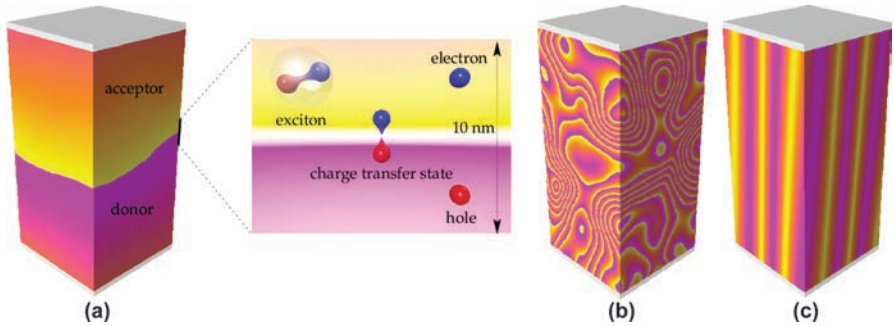

Figure 9.1 (a) Basic mechanisms of a solar cell function: exciton creation, diffusion, dissociation at the donor–acceptor interface; charge separation and diffusion towards the electrodes. (b) Morphology with a large surface/volume ratio and efficient charge separation. (c) Morphology with efficient charge transport towards electrodes in addition to efficient charge separation.

In an organic solar cell, for example, light absorption leads to the generation of excited, strongly-bound electron–hole pairs (excitons) (Figure 9.1a). To achieve substantial energy conversion efficiencies, these need to be dissociated into free charge carriers with a high yield. Free charge carriers, in turn, should be able to diffuse towards the electrodes such that they can be injected into an external circuit. Hence, to increase the efficiency of a solar cell, one should reduce the bandgap of the absorbing molecule (*e.g.* by using the donor–acceptor molecular architecture), engineer the level alignment at the heterojunction to have efficient splitting of Frenkel excitons into charge transfer states, and increase the charge mobility in the mesophases to reduce the non-geminate recombination. All of these processes are sensitive to the morphology of the blend (examples shown in Figure 9.1b,c).

Similarly, in a phosphorescent OLED, electrons and holes are injected into the transport layers *via* the electrodes, which ensures their balanced delivery to the emission layer (EML). To allow for triplet-harvesting, the EML consists of an organic semiconductor (host) doped by an organo-metallic emitter (guest). Excitation of the emitter can be achieved either by an energy transfer process, *i.e.* by the formation of an exciton on a host molecule and a subsequent energy transfer to the dopant, or by a direct charge transfer process. In the latter case, one of the charge carriers is trapped on the emitter and attracts a charge of the opposite sign, forming a neutral exciton on-site. This is argued to lead to more efficient OLEDs as compared to cases where excitation occurs by energy transfer. The goal is therefore to achieve a sufficiently fast charge/energy transport dynamics within the EML, while taking into account the interplay between the molecular electronic structure, the morphological order, and the relative alignment of the transport/excited state energy levels of the host and the guest.

Thus, it seems that a roadmap for the computer-based optimization of organic semiconductors is well-defined: One needs to predict the material's

morphology, calculate the energetic landscape for elementary excitations (*i.e.* charges and excitons), evaluate rates of various processes (*i.e.* charge/exciton transfer, geminate/non-geminate recombination), solve the time-dependent master equation, and analyze distributions of currents and occupation probabilities to extract/optimize measurable properties such as open-circuit voltage, short circuit current for solar cells, and color, efficiency, and lifetime for OLEDs. This would comprise a solution to the so-called ''forward'' (structure to property) problem. Repeating this procedure for a set of computer-generated compounds, these could then be pre-screened prior to their actual synthesis. One might even imagine the possibility of inverting the structure–property relationships by using machine-learning techniques and appropriate molecular descriptors.

In reality, however, the computer design of organic semiconductors has yet to reach this level of competence. In most cases, direct synthesis and characterization of a particular compound is still faster, easier and in most cases more reliable than computer-based predictions of its properties. The question is – Why? There are, in fact, several reasons for this. First of all, solving the forward problem is a non-trivial, interdisciplinary task (Figure 9.2), which requires the combined knowledge of quantum chemistry (molecular electronic structure, couplings, rates), statistical physics (self-assembly, drift-diffusion dynamics, optics), and engineering (device geometry, light in- and out-coupling).

Second, it is also a multiscale problem: On a molecular scale, every molecule has its own unique environment created by its neighbors with local

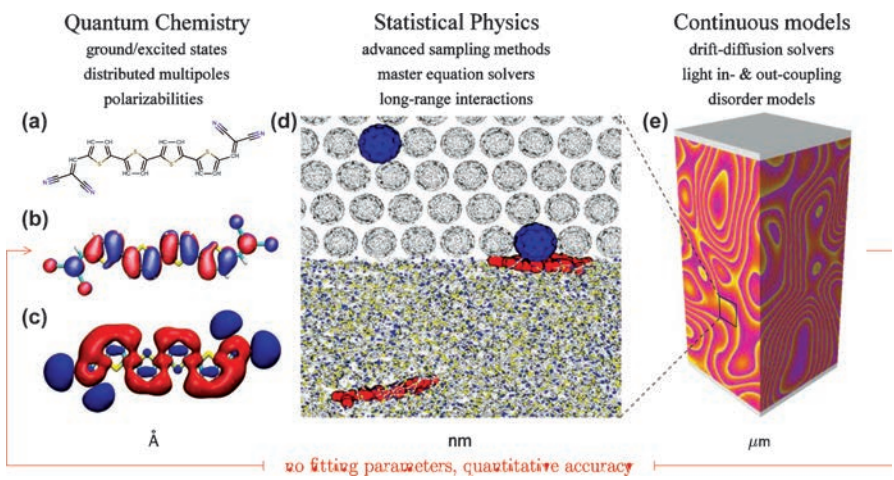

Figure 9.2 Multiscale nature of processes in organic materials. (a)–(c) Properties of isolated molecules used for accurate descriptions of electrostatic and polarization effects. (d) Simulations of large-scale atomistic morphologies using coarse-grained and force-field based models. Efficient solvers for the master equation with configuration-dependent rates. (e) Accurate parameterization of macroscopic descriptions.

electric fields leading to level shifts, broadening, and spatial correlations of charge/exciton energies. On a mesoscopic scale, the size of phase-separated domains of the donor and acceptor governs the efficiency of exciton splitting and charge percolation in a solar cell; the connectivity of the guest molecules in a host matrix determines the efficiency with which charges are delivered to the phosphorescent guest. In addition, on a macroscopic scale, light in–out-coupling needs to be accounted for to maximize absorption and emission. Likewise, the typical time scales of dynamic processes such as charge and energy transfer span several orders of magnitude. Hence, charge/exciton kinetics cannot be treated *via* numerical methods with a fixed time step, but rate-based descriptions must be employed instead.

Finally, to be predictive, the methods need to be quantitative. That is, not only each particular method is required to provide accurate values for the quantities of interest but the entire procedure of ''bottom-up scaling'' from the micro- to the macroscopic world should be robust. To illustrate this, let us focus on exciton and charge transport in a solar cell. Here, the energetic landscape is crucial for the excitation mobility. The main contributions to this landscape are from the (long-range) electrostatic interactions between the charged molecule and its environment, as well as excitation stabilization due to the polarization of its surroundings. To describe long-range interactions, cutoffs as large as 5–10 nm are required to accurately predict site energies. Systems of these sizes simply cannot be treated using first principles and an adequate classical representation needs to be employed. For excited states (*e.g.* Frenkel excitons), classical treatments alone are infeasible and QM/MM techniques are required. With the site energies at hand, one can evaluate the rates, which in general exponentially depend on site energy differences. This implies that all errors made when evaluating the energetic landscape will propagate into, for example, the charge mobility, exponentially. Therefore, an error propagation assessment at every level of parameter transfer is essential.

To this end, three distinct directions of modeling organic semiconductors have been pursued. At the most coarse level, *continuum* drift-diffusion equations have been employed to interpret experimental data, *e.g.* current–voltage characteristics.[1–3] This type of modeling is based on generic physical principles: only a few material-specific parameters, such as dielectric constants, charge carrier and exciton mobilities, diffusion constants, and creation/recombination rates, enter the equations. The continuum approach helps to analyze and optimize complex multilayered devices, but it by no means is limited to the device-engineering tasks. It can also be used to establish universal relationships between device parameters, for example the relation between the open-circuit voltage of a solar cell, the difference between the electron affinity and ionization potential of the acceptor and the donor materials, and the value of the short circuit current.[4,5]

The use of the continuum approach would not be possible without prior knowledge of charge/exciton diffusion constants, mobilities, injection barriers, *etc.* In organic semiconductors, these quantities have a non-trivial

dependence on the external field, the charge density, as well as the material's parameters. The generic expressions of these dependencies are often obtained by employing *mesoscale*-level descriptions. At the mesoscale, the electronic properties of single molecules and molecular pairs are coarse-grained into a few essential parameters, such as the hop attempt frequency, the hopping range, and the distributions and spatial correlations of the site energies. The morphological details are also ignored and regular lattices, potentially with a positional disorder, are used. The Gaussian-disorder family of models[6–12] has been particularly successful in providing analytical forms of these dependencies, helping to unveil the role of spatial correlations of the site energies on the field dependence of the charge mobility, as well as providing a unified description for mobility *versus* charge-carrier density for high and medium charge densities, achieved either in a field-effect transistor or a diode measurement.[13]

By construction, mesoscale models do not provide a direct link to the underlying chemical structure or material morphology. Moreover, model parameters must be extracted from experimental data, making material design and compound pre-screening virtually impossible. To remedy the situation, *microscopic* descriptions attempt to incorporate the molecular electronic structure and material's morphology into the charge/exciton transport models. A missing link between the micro- and mesoscales is normally introduced by employing more realistic charge/exciton transfer theories and by parameterizing the corresponding rates using first-principles calculations. This parametrization has to combine atomistic-level details of the material morphology with the information about the molecular electronic structure, and include accurate predictions of electrostatic and induction energies. Last but not least, efficient off-lattice master equation solvers with explicit Coulomb interactions must be used to study transport dynamics.

The aforementioned tasks are both computationally and methodologically challenging but definitely worth pursuing, as they help to establish the missing links between chemical structure, processing conditions, and the relevant macroscopic quantities of a device, *e.g.* open-circuit voltage in a solar cell or charge carrier distribution in an organic light emitting diode. Such links, or structure–property-processing relationships, help us to design new chemicals, optimize their processing, and enable compound pre-screening prior to their actual synthesis.

In what follows, we review the latest developments in microscale modeling of organic materials. This includes predictions of morphologies at an atomic level of detail (Section 9.2), charge/exciton transfer theories (Section 9.3.2), evaluation of electronic coupling elements (Section 9.3.3), site energies (Section 9.3.5), as well as methods required to solve the off-lattice master equation. Since the computational cost of microscopic approaches sets limits to accessible system sizes, special attention is paid to artifacts arising due to finite-size effects (Section 9.4), the truncation of long-range interactions (Section 9.6), and stochastic models which bridge the gap between the microscopic and mesoscopic worlds (Section 9.5).

9.2 Morphology Simulations

Let us first address the subject of the morphology. Molecular ordering in an organic semiconducting film can vary from completely amorphous to highly crystalline. The degree of ordering is often tunable by varying the chemical structure or processing conditions. In organic light emitting diodes, for example, where well-controlled homogeneous morphologies are required and high charge carrier mobilities are not essential, amorphous solids are used. As high charge carrier mobilities are needed in field effect transistors, single crystals or highly ordered polycrystalline films are employed. Similarly, in solar cells, high charge carrier mobilities in the donor and acceptor are required for efficient charge extraction. Excessive crystallinity can, however, be detrimental for the formation of a phase-separated morphology in a bulk heterojunction cell. In many cases, even ''highly crystalline'' organic semiconductors are only partially ordered in the active layer of a device. The morphological disorder can occur on different length scales, from local defects and grain boundaries to mixed amorphous/crystalline islands. Such morphological disorder can lead to energetic disorder (energetic traps) and large variations of electronic couplings (topological traps), hampering the transport of mobile charge carriers. To account for such effects, realistic models of molecular ordering must be capable of predicting the degree of molecular ordering, including the trap concentration. This is certainly one of the main challenges when it comes to modeling of morphologies at an atomistic level of detail. Another challenge is the supramolecular assembly of organic semiconductors: local molecular ordering coexists with large-scale heterogeneities, both equally important for efficient functionality. Thus, multiscale simulation techniques should be developed, capable of covering both length-scales, from ångströms to micrometers, as well as time-scales from femtoseconds to hours.

The theoretical and computational toolbox currently used to study self-assembling properties of organic materials is very versatile: On the highest level of resolution, it includes accurate quantum chemical calculations capable of predicting properties of isolated molecules. Less computationally demanding density functional methods can deal with much larger molecules and oligomers, including side chains, and are often used to compare ground state energies of experimentally proposed arrangements of atoms in a unit cell. To assess crystalline packing modes at ambient conditions and during annealing, as well as to study amorphous melts and longer chain lengths, classical force-fields are parametrized. To access even longer length- and time-scales (*i.e.* micrometers and microseconds) coarse-grained models are developed. The ultimate goal of these simulations is to self-assemble the compound *in silico*, *i.e.* to predict its polymorphs as well as the degree of disorder in the kinetically trapped molecular arrangements. The honest assessment, however, is that we are fairly far from achieving this goal. The main obstacles are the insufficient accuracy of the methods employed at a specific level of resolution, the long simulation times required to study

self-assembly, and the uncontrolled error propagation from one level to another, *e.g.* when parameterizing force-fields based on quantum chemical calculations or when developing coarse-grained models using force-field-generated reference data. In what follows, we summarize the available simulation techniques and point out which properties of single molecules and of molecular arrangements they are capable of providing.

9.2.1 First-Principles Calculations

Computationally demanding first principles calculations are mostly used to gain insight into the electronic structure, the ground state geometry of isolated molecules, and the properties of neutral periodic crystalline molecular arrangements. These calculations can, to some extent, serve as a guide for a qualitative understanding of properties of molecular assemblies. In the general case, however, processes in organic materials are extremely sensitive to the local molecular environment, the degree of long-range ordering, and the presence of defects and disorder. The results of first principles calculations should therefore be complemented by the environmental contributions. For computational efficiency, the latter are normally accounted for perturbatively, using classical force-fields. The parameters of these force-fields, *e.g.* distributed multipoles and polarizabilities, bonded and non-bonded interaction potentials, can also be obtained from first principles.[14–18]

However, first principles methods cannot be routinely applied in all cases, even for isolated organic molecules. A typical example here is the conjugated polymers (oligomers),[19–25] where the extended π-conjugation flattens the backbone, whereas the non-bonded interactions between consecutive repeat units (steric repulsions, Coulomb, and van der Waals interactions) often tend to distort the planarity. Typical energy differences between planar and non-planar conformations are of the order of 10 meV, which is the accuracy threshold of density functional methods. Hence, one is forced to use more accurate but computationally demanding quantum-chemical methods,[19] especially when parametrizing bonded interactions. At the same time, in conjugated polymers, the ground-state torsional angle between repeat units depends on the oligomer length and torsional potentials can be correlated up to a few nearest-neighbors.[25,26] This makes geometry predictions a formidable task, even for the case of isolated oligomers.

Another niche of research where first principles methods are employed is in studies of crystalline molecular arrangements. Here, density functional theory has been used to establish whether experimentally reported crystal structures correspond to well-defined energy minima.[23,27–29] Since the van der Waals interaction provides one of the major contributions to the cohesive energy of a crystal, density-functional approaches have to be complemented by either *ad hoc* terms[30,31] or using semi-classical approaches.[16,32,33] Similar to the situation with a single isolated chain, typical energy differences between diverse packing motives are of the order of

10 meV per unit cell and, hence, theoretical methods are at their accuracy limits, making it difficult to rank the different molecular arrangements. Note, that unit-cell optimizations and free energy estimates are often performed at 0 K, and so entropic effects are ignored.

Apart from force-field parameterizations, formation energies, and densities of states of crystalline arrangements, first principles methods can also be used to evaluate some of the ingredients of charge and exciton transfer rates and, in general, to study chemical reactions occurring upon the oxidation, reduction, and excitation of organic molecules. Representative examples are evaluations of electronic coupling elements between diabatic states (discussed in more detail in Section 9.3.3), reorganization energies (Section 9.3.4), and electron affinities and ionization potentials of isolated molecules. They are also imperative for identifying localized states in polymeric systems, where both strong and weak electronic couplings coexist in the same molecule and simple criteria for conjugation segments cannot be identified (Section 9.3.1). Finally, first principles methods can be used to parametrize model Hamiltonians, which are solved when charge transfer and nuclear dynamics occur on a similar timescale, or when nuclear dynamics are not harmonic and the analytical expression for the transfer rate is not available.[34–39] These approaches are discussed in more detail in the contribution of Ortmann, Radke, and Cuniberti in this book (Chapter 8).

9.2.2 Atomistic Models

To study larger systems and longer time-scales, various types of force fields are developed. These integrate out electronic degrees of freedom and operate with the (many-body) interaction potential between nuclei. The potential is used to propagate classical equations of motion, sample the phase space of the system in a specified ensemble, and evaluate averages of macroscopic observables. The basis functions used to represent the potential energy surface are often chosen according to chemical intuition and split into bonded (bonds, angles, torsions) and non-bonded (van der Waals, Coulomb) contributions, for which simple analytical expressions or tabulated functions can be used. A detailed overview of this classical approach can be found in several original works as well as textbooks.[16,40–42]

For the sake of computational efficiency, induction effects (molecular polarizabilities) are implicitly incorporated by adjusting partial charges and van der Waals interactions. Parametrizations of effective charges and Lennard-Jones parameters require experimental input such as transition temperatures, density, and other thermodynamic properties, and are often performed for a specific state point and a mesophase. Transferability to other compounds (*e.g.* from biological systems to organic semiconductors) is not guaranteed. The most common re-parametrization includes the adjustment of the equilibrium values for bond lengths and angles, the fitting torsional potentials to *ab initio* calculations, and the reparametrization of partial charges using the electrostatic potential fits of an isolated molecule.

A representative example is the gradual refinement of the P3HT force-field, where parameters of an existing force-field have first been refined in order to reproduce the torsional potential between thiophene units and electrostatic potential around an isolated oligomer[43,44] and, subsequently, to account for the change in the backbone potential with increasing oligomer length.[20,22,24,44–46]

A more computationally demanding, *polarizable* force-field incorporates induction effects *via* distributed polarizabilities and includes higher multipoles in the description of electrostatics. As such, it rigorously accounts (in a perturbative way) for electrostatic, induction,[14] and van der Waals[16] interactions on the same footing. Since all parameterizations can be performed from first principles, it is the only method that can be used for systematic pre-screening of new compounds. In large systems, however, the evaluation of induced dipoles requires a self-consistent solution of coupled non-linear equations, which is computationally demanding. Thus, in practice, such large-scale morphologies are simulated using standard (or adjusted) force-fields while site energies required for the evaluation of rates are computed using polarizable force-fields.[47–49]

Three typical examples of employing classical force-field simulations to analyze or even predict molecular alignment of organic semiconductors are shown in Figure 9.3: Figure 9.3(a) depicts lamellar arrangement of the conjugated polymer, regioregular P3HT,[44,50] obtained by equilibrating the experimentally known crystal structure of the P3HT polymorph I. Notably, even with these, classical descriptions, only highly crystalline morphologies and high-temperature amorphous melts can be studied. Figure 9.3(b) shows the vacuum-deposited layer of a small-molecule organic dye (DCV5T) on top of crystalline C_{60}, which assembles into a glassy phase with nematic ordering. Finally, Figure 9.3(c) shows an amorphous host/guest system generated by thermal annealing of a binary mixture of two organic compounds used in the active layer of an OLED.[51,52]

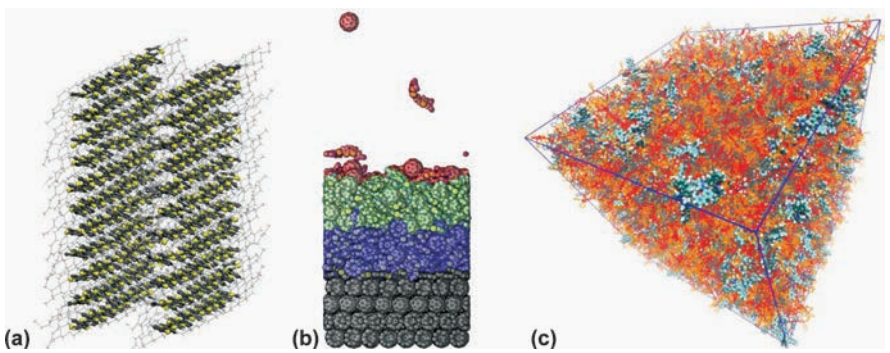

Figure 9.3 (a) Lamellar molecular arrangement of regioregular P3HT; (b) bulk heterojunction solar cell (C_{60} : DCV5T) simulated by depositing single molecules of C_{60} and DCV5T on top of a C_{60} crystal; (c) amorphous host–guest system of an active layer of an OLED.

9.2.3 Coarse-Grained Models

In many cases, not only local but also large-scale material ordering is essential for a functional device. Single grains in field-effect transistors or domain sizes of the donor and acceptor materials in a solar cell can, for example, be as large as several hundreds of nanometers. At the same time, the time-scales involved in some of the stages of material processing (solvent evaporation, annealing) can range anywhere from seconds up to hours. Such length- and time-scales cannot feasibly be reached by atomistic molecular dynamics simulations. One can, however, explore the fact that certain parts of the system evolve on much slower times and larger length-scales (*e.g.* a thiophene ring rotation in a polythiophene occurs on a much slower time-scale than a characteristic bond vibration). One can therefore combine several coherently moving atoms, connected *via* fast degrees of freedom (*e.g.* bonds), into a single interaction site. By doing this, we reduce the number of degrees of freedom to be propagated and, more importantly, obtain a much smoother potential energy landscape in terms of the coarse-grained degrees of freedom (softer interaction potentials, less friction), allowing one to simulate ten to hundred longer times and system sizes.

The coarse-graining procedure in itself involves three steps: choice of the coarse-grained degrees of freedom, identification of a merit function (norm), which quantifies the difference between the fine- and coarse-grained representations, and determination of the coarse-grained potential energy surface (PES). The entire procedure can be thought of as a projection of the fine- onto the coarse-grained PES and is therefore sensitive to the number and types of basis-functions employed in the CG representation. In practice, these are limited by the functional forms included in the coarse-grained force field, which usually exclude many-body contributions. To perform correct statistical sampling of the coarse-grained degrees of freedom, the potential of mean force should be used as their interaction potential,[54] which is inherently a many-body potential. The accuracy of the coarse-grained model thus becomes sensitive to the way the projection is performed as well as the number of basis functions that are used to represent the coarse-grained force-field.[55] Existing projection schemes either try reproducing various pair distribution functions (structure-based coarse-graining[56–59]), matching the forces,[54,60,61] minimizing the information loss in terms of relative entropy,[62] or using liquid state theory.[63] An extensive overview of such coarse-graining techniques is provided in ref. 64.

In the field of organic semiconductors, one of the most challenging tasks is to quantify the self-organizing abilities of a material solely based on its chemical structure. Relevant self-assembled structures in this field are lamellar arrangements of conjugated polymers, partially crystalline phases of a small-molecule donor/acceptor material, or molecular alignments at the interface between the organic layers. Since these require systems on the order of (hundreds of) thousands of molecules, various coarse-grained models have been developed.[65–69]

A typical example of a coarse-grained model is the three-site model developed for P3HT. Here, the P3HT monomers are coarse-grained into three interaction sites placed at the center-of-mass of each of the thiophene rings and on every three methyl groups of the hexyl side-chain. This model is capable of reproducing the lamellar molecular arrangements of P3HT, as well as the phase separation observed in P3HT/PCBM blends.[68,70]

Often, the accuracy of the coarse-grained model can be improved by explicitly incorporating information about macroscopic properties of the system, *i.e.* its equation of state or the symmetry of its mesophase.[71,72] Moreover, one can further reduce the number of degrees of freedom by introducing anisotropic interaction potentials. An example of such a model with soft interaction potentials is shown in Figure 9.4. Here, all of the non-bonded interactions are chosen such that the system has a desired phase behavior (biaxial nematic to nematic to isotropic phase transition) while all of the torsion and dihedral angle distributions reproduce those of the underlying isolated atomistic chain in θ-solvent conditions.[53] Using this model, one can equilibrate systems as large as $50\times50\times50$ nm^3, containing 5×10^5 chains with 32 monomers per chain. The model predicts reasonable values for the persistence length and Frank elastic constants and also provides some insight into how the collective orientation of backbones affects the energetic landscape for drift-diffusion of charges, which turns out to be spatially correlated even without taking long-range Coulomb interactions into account.

Finally, the most coarse models for morphology simulations employ field-theoretical descriptions, *e.g.* the self-consistent field theory method with the Flory–Huggins Cahn–Hillard functional. The bulk heterojunction morphologies,[73–77] generated by this method, can be used as input for either a self-consistent solution of the continuity-transport equations for electrons, holes, and excitons in conjunction with Poisson's equation[73,76–79] or they can be coupled to a suitable kinetic Monte Carlo algorithm.[74,75,80] These approaches help us to study the effect of boundary conditions on

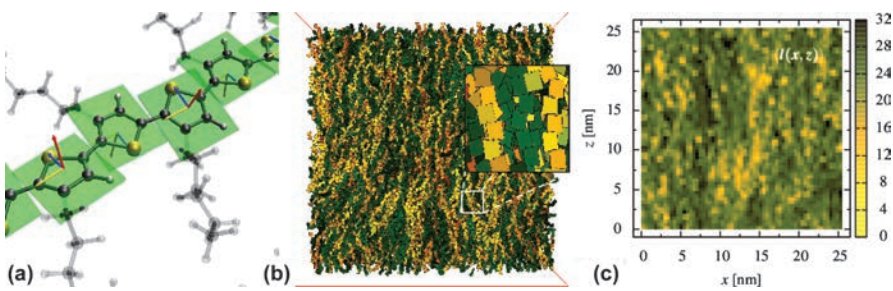

Figure 9.4 (a) Atomistic and coarse-grained representation of a P3HT side chain. (b) Biaxial nematic alignment in a melt of P3HT chains. (c) Spatially-correlated distribution of conjugation segments, leading to a correlated energetic landscape.
Adapted with permission from ref. 53. Copyright (2013) American Chemical Society.

self-assembly and orientation of lamellar phases, as well as the influence of the degree of phase separation and ordering on the photovoltaic device characteristics.

9.3 Charge Transport

We will now discuss the simulation techniques used to assess semiconducting properties of organic materials, in particular the charge carrier mobility. Since a first-principles-based analysis of non-equilibrium electron transport in these materials is computationally infeasible, one has to decide upon an appropriate model for charge transport, or a model Hamiltonian. For perfectly ordered crystalline organic semiconductors, the Drude model based on band theory is often used, where the charge mobility is determined from the mean relaxation time of the band states and the effective mass of the charge carrier.[81–83] Such band-based models can be further extended to account for electron–phonon coupling.[34,39,84] At ambient conditions, however, the thermal fluctuations of the non-local electron–phonon coupling or the transfer integral can become of the same order of magnitude as its average value, such that charge transport becomes diffusion-limited by thermal disorder. The corresponding description (semiclassical dynamics) can be achieved by using a Hamiltonian with interacting electronic and nuclear degrees of freedom.[38] If the nuclear dynamics are much slower than the dynamics of the charge carrier while the electronic coupling is weak, a Hamiltonian with a static disorder is assumed with an electronic density of localized states and hopping rates between them. The latter approach is often used to study amorphous and partially ordered small-molecule-based organic semiconductors. Hopping rates can be postulated empirically as in the Gaussian disorder models[8] or evaluated from quantum-chemical calculations and combined with various charge transfer theories as discussed in Section 9.3.2.

The appropriate description for a particular material model is often predetermined by experiment. For example, an increase in the mobility with rising temperature is often interpreted as a sign of *temperature-activated hopping* transport, with localized charges (charged states) and thermally activated (sometimes tunneling-assisted) charge transfer reactions. Charge localization allows one to cast charge transport as a series of charge transfer reactions. If the charge transfer rates of these reactions are known, the resulting master equation for the occupation probabilities of localized states can be used to study charge dynamics in the system. The solution to the master equation provides information about the charge distribution and currents, and eventually the mobility, all as a function of temperature, the external field, the charge density, and, importantly, the underlying morphology. In what follows, we first introduce the quantities necessary for describing charge transfer reactions, then discuss the simulation techniques required for their evaluation, and finally illustrate how to solve the master equation to obtain the charge carrier mobility.

9.3.1 Diabatic States

The first-principles description of a charge transfer, or an oxidation–reduction reaction, of type $A^{-}B \rightarrow AB^{-}$ can be obtained by analyzing solutions to the Schrödinger equation with a dimer Hamiltonian:

$$\hat{H} = \frac{\hbar^2}{2m_e}\sum_i \nabla_i^2 - \sum_{i,I}\frac{Z_I e^2}{|\vec{r}_i - \vec{R}_I|} + \frac{1}{2}\sum_{i\neq j}\frac{e^2}{|\vec{r}_i - \vec{r}_j|} - \sum_I \frac{\hbar^2}{2M_I}\nabla_I^2 + \frac{1}{2}\sum_{I\neq J}\frac{Z_I Z_J e^2}{|\vec{R}_I - \vec{R}_J|}, \tag{9.1}$$

where the nuclei of a dimer AB with charges $Z_I e$ and masses M_I are located at positions $\vec{R}_I$ and electronic coordinates are denoted as $\vec{r}_i$. A practical way of solving this equation is to introduce the Born–Oppenheimer approximation, which assumes that electronic motion in a specific state of a system occurs on significantly faster time-scales than the motion of the nuclei. This allows one to separate the electronic and nuclear degrees of freedom and to solve the electronic Hamiltonian, assuming a parametric dependence on the nuclear degrees of freedom. The solution of the electronic Hamiltonian, that is, a set of orthogonal *adiabatic* states $\phi_\nu(\vec{r};\vec{R})$, can be used to expand the molecular wavefunction:

$$\psi(\vec{r};\vec{R}) = \sum_\nu \chi_\nu(\vec{R})\varphi_\nu(\vec{r};\vec{R}) \tag{9.2}$$

After substituting this expansion into the Schrödinger equation, we obtain a set of coupled equations for $\chi_\nu(\vec{R})$. The (non-adiabatic) coupling between the adiabatic states, which is mediated by the nuclear kinetic energy operator, is referred to as *dynamic coupling*. Its calculation requires knowledge of the first and second derivatives of the electronic wavefunction. In addition, the electronic wavefunction can change rapidly during the charge transfer reaction, implying that this coupling can be singular within a narrow range of nuclear configuration space, leading to numerical complications. To summarize, adiabatic functions are useful as long as non-adiabatic couplings can be neglected, *i.e.* when charge transfer occurs within a single electronic state driven by a slow nuclear reaction coordinate.

In practice, it is, however, convenient to use *diabatic* basis functions φ_ν, which are eigenstates of the electronic Hamiltonian, evaluated at some fixed nuclear configuration $\vec{R}_0$. Expanding the wavefunction in this basis, we again obtain a set of coupled linear equations but now the couplings are not mediated by the non-adiabaticity operator. This is because diabatic basis functions do not depend on $\vec{R}$ but are shifted from the kinetic to the potential energy operator. In general, any complete basis set that solves the stationary Schrödinger equation and yields negligible small matrix elements of the nonadibaticity operator can be used. An example of this is a so-called ''frozen-core'' approximation, where the diabatic states of a dimer are

constructed from the frontier orbitals of (neutral) isolated monomers[85–88] and it is assumed that the reduction/oxidation of a monomer does not alter the rest of the orbitals. Another option is to use the constrained density-functional theory, where a density constraint is applied, forcing the charge to localize on the individual monomers of the dimer.[89] Note that more computationally demanding approaches have also been proposed.[90–101]

Determining the diabatic states in polymeric systems is another important area of computational studies that deserves special attention. Indeed, in the case of small molecules or relatively short oligomers, one can often assume that the charge is localized on the entire molecule. In polymers, however, it has been proposed that the charge localizes on molecular (conjugated) segments or regions between conjugation breaking, where strong deviation from planarity occurs.[47,102] This idea has been used to interpret spectroscopic data, but is difficult to justify when wanting to rigorously define a sharp threshold that separates complete conjugation breaking from full conjugation between oligomers. Moreover, many polymers form crystalline domains that are so extended that no conjugation breaks occur for nanometers[103] but the charge is certainly more localized than that, either due to the disorder present in the semicrystalline phase or the electron–phonon coupling.[104,105]

Hence, to determine the charge localization, there is no other alternative than computing the electronic wavefunction of a large model system that is generated by classical simulations. The excited state of the charged simulation box cannot be computed with modern computational methods and therefore it becomes impossible to even evaluate the nuclear relaxation (reorganization energy) for the hopping between two states. For these reasons, all attempts to evaluate the wavefunction of a large model of polymers have focused on neutral systems and have so far interpreted only the one-electron states (molecular orbitals) as possible sites where the excess charge can be localized.[36,106] Results are normally presented in terms of the density of states (DOS) and localization length, although it should be noted that the two quantities should only be used for systems with orbitals fully filled and empty above and below the band gap. Such descriptions are also not directly comparable with the models in Section 9.3.2, which take into account electron and nuclear polarization, but have to make assumptions for the localization length.

For the one-electron states to be representative of the actual localization of the charge carrier, a further condition needs to be satisfied. The charge needs to be localized predominantly by the conformational disorder of the polymer and not by the electron–phonon coupling. If the electron coupling is particularly strong, the frontier orbitals may be delocalized over many monomers. However, when an excess charge is added, the nuclear polarization will localize the charge, completely modifying the electronic wavefunction with respect to the neutral calculation. Calculations for, *e.g.* P3HT, support this approximation[36,107] but it should be noted that polaron sizes are heavily dependent on the DFT methodology[108] and that the same assumption might not hold for new families of semiconducting polymers[109]

in which large conjugated units are more weakly coupled by smaller conjugated linkers. In general, if the polaron size of a perfectly ordered system is much larger than the orbital in the disordered model, it is acceptable to determine the charge localization from calculations that neglect the electron–phonon coupling as a first approximation. Again, for P3HT, there is a consensus that the localization of the wavefunction largely originates from the disorder and not the electron–phonon coupling, since there is a correlation between the increased order of P3HT and increased mobility.[110–112]

Assuming that the calculation of a ground state wavefunction of a polymer model yields information about the charge localization for the carrier states, it is still not trivial to carry out such calculations. It is not obvious to know in advance how large should a model of bulk polymer be to reproduce the DOS and localization length without the results being affected by finite size effects. The experience of available calculations with P3HT and PPV suggests that a model containing several chains of 20 to 40 monomers displays electronic properties that do not depend appreciably on the chain length[113] (it should not be forgotten though that the morphology depends on the chain length until much larger molecular weight.[114]) Such models will contain tens of thousands of atoms, a number still one order of magnitude larger than what is normally achievable by the current software specialized in linear scaling *ab initio* calculations.

However, many ideas of linear scaling methodology can be used to develop *ad hoc* methods that are able to compute in more approximate fashion the wavefunction for large systems by using a very localized basis set that reduces the number of matrix elements to be evaluated.[115–117] Different schemes have been proposed to evaluate the diagonal and off-diagonal elements of such reduced Hamiltonian, including a fragment molecular orbital approach[118] and a charge patching method.[106,119,120] General formalism for such methods have been developed by the quantum chemistry community.[115,121–123]

The various partitioning schemes proposed for polymer systems are very often complemented by further approximations that take into account the chemical structure of the investigated system. As the frontier orbitals are invariably localized on the conjugated fragment of the monomer, while a large fraction of the molecular weight is taken up by the polymer side chains that do not contribute to the charge transport states, it is customary to remove the side chains in the calculation, sometimes substituting them with effective point charges that simulate the missing electrostatic effects.[113] For lamellar systems (such as P3HT and PBTTT) it is a good approximation to neglect the electronic coupling between lamellae, thereby describing a system that is essentially two-dimensional.[36,124] An alternative approach to full or *ad hoc* linear scaling DFT methods is the calculation through approximate DFT methods such as the tight binding DFT.[125] This family of methods has been developed over the years and the most convenient version of the methodology is the self-consistent charge-density functional tight binding.[126] One–two order of magnitudes acceleration of the electronic

structure calculation can be achieved by an approximate evaluation of the Kohn–Sham–Fock matrix elements in the atomic orbital basis. A very broad range of applications apart from organic semiconductors have been proposed[123] but relatively few have been reported for semiconducting polymers.[127] Finally, an obvious choice for the calculation of electronic structure on large scale systems would be by semi-empirical methods. These have been the method of choice for many years to explore charge- and exciton-dynamics[128,129] in single chain polymers containing carbon atoms but there are very few systematic studies on their reliability for polymers containing heteroatoms.

Once the one-electron states of a large system have been evaluated, it is still challenging to derive a master equation (Section 9.3.6) that describes the transitions between these states. Vukmirović and Wang have proposed a perturbative expression assuming that these states are coupled by non-adiabatic coupling terms that can be evaluated explicitly[106] or approximated using the overlap between the absolute value of the wavefunction.[130] The proposed expression does not contain the effect of nuclear reorganization in the presence of an additional charge and is valid only in the limit of vanishing reorganization energies, like in the Miller–Abrahams rates.[131] Using this approach, it has been highlighted that the DOS does not contain all of the information needed to evaluate the mobility and that it is possible to have reduced broadening of the DOS due to increased order but still have low mobility because of the coupling between the states is reduced.[132] Alternative methods to combine nuclear polarization and disorder effects have been proposed, but these could so far only be applied to simple model systems.[133,134] An extended discussion of charge delocalization in polymeric systems is provided in ref. 135.

9.3.2 Charge Transfer Rates

The simplest rate expression for a charge transfer reaction can be derived for a system with classical harmonic vibrational degrees of freedom or the high-temperature limit.[136,137] The diabatic and adiabatic potential energy surfaces of a dimer are shown in Figure 9.5. The corresponding rate expression reads:

$$k_{A\to B} = \frac{2\pi}{\hbar}\frac{J_{AB}^2}{\sqrt{4\pi\lambda kT}}\exp\left[-\frac{(\Delta U_{AB}-\lambda)^2}{4\lambda kT}\right] \tag{9.3}$$

This so-called Marcus-rate depends only on three microscopic parameters, namely, the reorganization energy λ, the electronic coupling J_{AB}, and the driving force $\Delta U_{AB} = U_A - U_B$, all of which can be evaluated using quantum-chemical methods, classical polarizable force-fields, or quantum-classical hybrid methods, as discussed in the following sections.

Note that both classical and semi-classical expressions for charge transfer rates are often criticized as being not applicable for studying charge

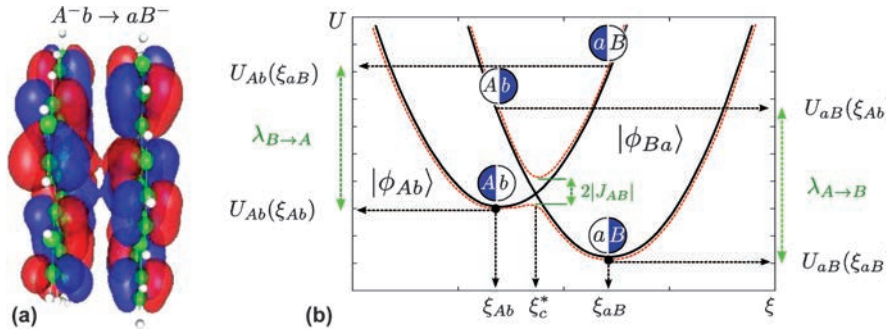

Figure 9.5 (a) Diabatic states constructed using the molecular orbitals participating in a charge transfer reaction (frozen core approximation). (b) Diabatic (solid black line) and adiabatic (dashed red line) potential energy surfaces of two electronic dimer states $|\varphi_{AB}\rangle$ and $|\varphi_{aB}\rangle$, participating in the charge transfer reaction $A^-B \rightarrow AB^-$ along the reaction coordinate ξ.

transport in well ordered organic semiconductors. Having said this, one has to also acknowledge that, so far, it is the only way of linking a large-scale morphology to the charge dynamics in partially disordered materials. Of course, this should not serve as an excuse for not validating the Marcus expression (or its quantum equivalent) for the charge transfer rates. In fact, various generalizations of this expression to quantum-mechanical modes have been derived.[138–140] Moreover, indications that these expressions are better suited for describing charge transport, especially at low temperatures and high fields, have recently been reported.[141]

9.3.3 Electronic Coupling Elements

Electronic coupling elements, or transfer integrals, between molecules i and j are given by the off-diagonal matrix elements[99,137]:

$$J_{ij} = \left\langle \phi_i | \hat{H} | \phi_j \right\rangle \tag{9.4}$$

where $\phi_{i,j}$ are the diabatic states often approximated by the frontier orbitals of the molecules, and $\hat{H}$ is the dimer Hamiltonian. These quantities are normally evaluated using electronic structure theory. Expanding the adiabatic states of the dimer into monomer states produces the following secular equation:

$$(\mathbf{H} - E\mathbf{S})\mathrm{C} = 0 \tag{9.5}$$

where $\mathbf{H}$ and $\mathbf{S}$ are the Hamiltonian and overlap matrices of the system:

$$\mathbf{H} = \begin{pmatrix} e_i & H_{ij} \\ H_{ij}^* & e_j \end{pmatrix}, \mathbf{S} = \begin{pmatrix} 1 & S_{ij} \\ S_{ij}^* & 1 \end{pmatrix} \tag{9.6}$$

and the eigenfunctions:

$$e_i = \left\langle \phi_i \mid \hat{H} \mid \phi_j \right\rangle,\ e_j = \left\langle \phi_j \mid \hat{H} \mid \phi_i \right\rangle,\ H_{ij} = \left\langle \phi_i \mid \hat{H} \mid \phi_j \right\rangle,\ S_{ij} = \left\langle \phi_i \mid \phi_j \right\rangle$$

In the basis of its eigenfunctions, the Hamiltonian operator is diagonal, $\left\langle \varphi_n^D | \hat{H} | \varphi_m^D \right\rangle = E_n \delta_{nm}$. Hence, eq. (9.5) can be rewritten as:

$$H_{ij} = \sum_n \left\langle \phi_i | \phi_j^D \right\rangle E_n \left\langle \phi_{n_i}^D | \phi_j \right\rangle \tag{9.7}$$

Expanding the monomer and dimer functions into a basis set of atom-centered orbitals:

$$|\phi_k\rangle = \sum_\alpha M_\alpha^{(k)} |\varphi_\alpha\rangle,\ |\phi_n^D\rangle = \sum_\alpha D_\alpha^{(n)} |\varphi_\alpha\rangle$$

the projections read as:

$$\left\langle \varphi_i | \varphi_n^D \right\rangle = \sum_n M_\alpha^{(k)} \left\langle \alpha | \sum_\beta D_\beta^{(n)} | \beta \right\rangle = \boldsymbol{M}_{(k)}^\dagger \mathscr{S} \mathbf{D}_{(n)} \tag{9.8}$$

where $\mathscr{S}$ is the overlap matrix of the atomic basis functions. The Hamiltonian and overlap then take the form:

$$H_{ij} = \overline{\boldsymbol{M}}_{(i)}^\dagger \mathscr{S} \mathbf{D} \mathbf{E} \mathbf{D}^\dagger \mathscr{S}^\dagger \overline{\boldsymbol{M}}_{(j)} \tag{9.9}$$

$$S_{ij} = \overline{\boldsymbol{M}}_{(i)}^\dagger \mathscr{S} \mathbf{D} \mathbf{D}^\dagger \mathscr{S}^\dagger \overline{\boldsymbol{M}}_{(j)} \tag{9.10}$$

The final required transformation is the diagonalization of the diabatic states imposed by the charge-transfer Hamiltonian.[142] An orthonormal basis set that retains the local character of the monomer orbitals can be obtained by using the Lödwin transformation, $\mathbf{H}^{\text{eff}} = \mathbf{S}^{-1/2} \mathbf{H} \mathbf{S}^{-1/2}$, yielding an effective Hamiltonian with its entries directly related to the site energies ε_i and transfer integrals J_{ij}:

$$\mathbf{H}^{\text{eff}} = \begin{pmatrix} \varepsilon_i & J_{ij} \\ J_{ij}^\star & \varepsilon_j \end{pmatrix}. \tag{9.11}$$

The projection method can be significantly simplified if semiempirical methods are employed for the dimer Hamiltonian[85–87] as well as made computationally more efficient by avoiding self-consistent dimer calculations.[88] Notably, the density functional and semiempirical methods can introduce a systematic error when used to evaluate electronic couplings.[140,142]

As the electronic coupling and, correspondingly, charge carrier mobility is intimately related to molecular overlap, it is very sensitive to relative positions and orientations of neighboring molecules. To illustrate this, Figure 9.6 (left-hand side) shows the absolute value of the electronic coupling element as a function of the azimuthal rotation angle for several

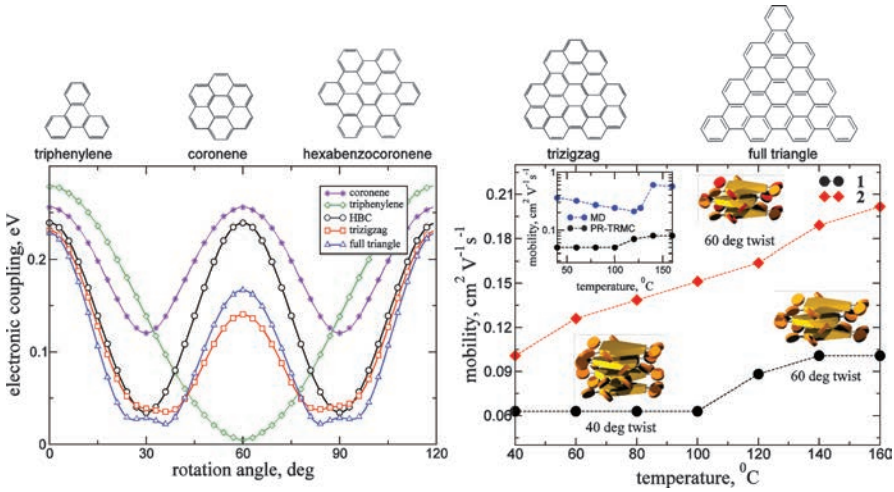

Figure 9.6 (Left-hand side) Absolute values of the electronic coupling element as a function of the azimuthal rotation angle for several symmetric polyaromatic hydrocarbon cores. The separation was fixed to 0.36 nm. (Right-hand side) Charge mobilities as a function of temperature as measured by the PR-TRMC technique. Inset: direct comparison to simulation. Adapted with permission from ref. 143. Copyright (2009) Macmillan Publishers Limited.

polyaromatic hydrocarbons. Here, the most favorable molecular arrangement is either co-facial or twisted by 60° (except triphenylene). For efficient charge transport, it is therefore preferable to lock the relative molecular orientations at the positions of the maxima of the transfer integral, which can be achieved by adjusting the density and type of side chains.[143]

This example shows that it is in principle possible to predict the optimal molecular arrangement for charge transport. This description, however, relies on a static picture, whereas in reality electronic couplings are time-dependent. To understand whether a static picture can be employed, one has to compare the distributions of the relaxation times of the electronic coupling elements and site energies to the distributions of the escape times of a charge carrier. For instance, for P3HT, even the slowest escape times for holes do not extend into the decorrelation regime of the electronic couplings. Charge-carrier dynamics are therefore limited by the static disorder of the electronic couplings, since their relaxation times exceed typical timescales of hopping transport. Hence, it is possible to resort to a single charge-transfer rate without time-averaging of electronic couplings of a pair of molecules.[44] The reason for the slow relaxation times of electronic couplings is the chemical structure of P3HT: every thiophene unit is linked to an alkyl side-chain with slow dynamics, both in the crystalline and amorphous phases. This overdamps the backbone dynamics, in particular the torsional motions of the thiophene units, and results in slow variations of the electronic couplings. Interestingly, in a very similar conjugated polymer PBTTT,

where the thienothiophene units are not linked to the side-chains (implying a lower side-chain density and higher crystallinity), electronic couplings have significantly faster dynamics, which is beneficial for charge transport.[44,144,145]

9.3.4 Reorganization Energies

The internal reorganization energy is a measure for how much the geometry of the charge transfer complex adapts while the charge is transferred. The reorganization energy can be estimated based on four points on the diabatic potential energy surfaces (PES) (Figure 9.5):

$$\begin{aligned}\lambda_{A\to B} &= U_a(\xi_A) - U_a(\xi_a) + U_B(\xi_b) - U_B(\xi_B),\\ \lambda_{B\to A} &= U_b(\xi_B) - U_b(\xi_b) + U_A(\xi_a) - U_A(\xi_A)\end{aligned} \tag{9.12}$$

Here, $U_{a,b}$ and $U_{A,B}$ refer to the diabatic states of molecule A,B in their neutral and charged state, respectively. Treatments that do not approximate the PES in terms of a single shared normal mode are also available,[47,137,146]

An additional contribution to the overall λ results from the reorganization of the environment in which the charge transfer takes place, giving rise to λ^{out}. In a classical case, this outer-sphere reorganization energy contributes to the exponent in the rate expression in the same way as its internal counterpart. Assuming that charge transfer is significantly slower than electronic polarization but much faster than nuclear the rearrangement of the environment, λ^{out}, can be evaluated from the electric displacement fields created by the charge transfer complex,[137] provided that the Pekar factor is known. It also turns out that the classical Marcus expression for the outer-sphere reorganization energy (inversely proportional to the molecular separation) can predict negative values of λ^{out} for small intramolecular separations, which is unphysical and hence shall be used with care.[140]

For a P3HT chain of 20 monomers, the reorganization energy of 0.1 eV is relatively small compared to the 0.2–0.4 eV observed in many small-molecule based organic semiconductors due to the better delocalization of the charge. Additionally, steric hindrance prevents conformational changes of the polymer chain upon charging if embedded in a π-stacked crystal, since the resulting constraint on the backbone planarity lowers the reorganization energy.[147]

9.3.5 Driving Forces

The energetic landscape, that is, the change in the system's energy when a charge or exciton is drift-diffusing in an organic material, is one of the most crucial quantities affecting a device's functionality. In solar cells, for example, it assists the splitting of the Frenkel excitons into charge transfer states (and consequently into free charges), as well as influences the charge and exciton mobility and diffusion constants. In OLEDs, it is possible to

force charge carriers to form an exciton on a specific molecule (phosphorescent guest) by adjusting the energetic landscape.

For every molecular pair, the free energy difference (or *driving force* ΔU_{AB}) is given by the difference in *site energies* $U_A - U_B$, that is, the energy separation between the diabatic PES minima as shown in Figure 9.5. The latter include an internal contribution U^{int}, namely, the electron affinities for electrons and ionization potentials for holes of isolated molecules. U^{int} can vary from one molecular pair to another because of different energy levels for different types of molecules, or different conformers of the same molecule. The external contribution is due to the electrostatic, U^{est}, and the induction, U^{ind}, interactions of a charged/excited state with the environment:

$$\begin{aligned} U_A &= U_{Ab}(\xi_{Ab}) - U_{ab}(\xi_{ab}) = \left(U_{Ab}^{\text{int}} - U_{ab}^{\text{int}}\right) + \left(U_{Ab}^{\text{est}} - U_{ab}^{\text{est}}\right) + \left(U_{Ab}^{\text{ind}} - U_{ab}^{\text{ind}}\right) \\ U_B &= U_{aB}(\xi_{aB}) - U_{ab}(\xi_{ab}) = \left(U_{aB}^{\text{int}} - U_{ab}^{\text{int}}\right) + \left(U_{aB}^{\text{est}} - U_{ab}^{\text{est}}\right) + \left(U_{aB}^{\text{ind}} - U_{ab}^{\text{ind}}\right) \end{aligned} \tag{9.13}$$

Here, the subscript *ab* denotes the reference (neutral) state of the system, with all molecules being in their ground states.

It is the interaction with the environment that is the most difficult to evaluate: since the underlying interactions are long-ranged, large system sizes are needed to converge the values of site energies. To self-consistently account for both the electrostatic and the polarization effects, classical models are normally employed such as the polarizable force-fields. These models are computationally demanding (despite being classical) and are often not accurate enough when used ''out of the box''. For example, the Thole model, which performs extremely well for biomolecular systems, can easily underestimate the anisotropy of a molecular polarizability tensor for an extended π-conjugated system.

9.3.5.1 *Electrostatic Contribution*

The electrostatic interaction energy in the site-energy calculation can be evaluated as the first-order energy correction term, which stems from treating an external field as a perturbing term in the molecular Hamiltonian. This term is normally evaluated using atomic distributed multipoles, where the interaction energy U_{AB} of two molecules *A* and *B*, located at positions $\vec{X}$ and $\vec{Y}$, reads:

$$U_{AB} = \frac{1}{4\pi\varepsilon_0} \int\int \mathrm{d}^3x \mathrm{d}^3y \frac{\rho_A(\vec{x})\rho_B(\vec{y})}{|\vec{Y} + \vec{y} - \vec{X} - \vec{x}|} \tag{9.14}$$

Here ρ_A and ρ_B are charge densities of molecules *A* and *B*, respectively.

Using the spherical-harmonic addition theorem,[14] this energy can be re-written in terms of the molecular multipole moments, defined with respect to the molecule's local frame:

$$U_{AB} = \frac{1}{4\pi\varepsilon_0} \sum_{l_1,l_2} \sum_{k_1,k_2} \begin{pmatrix} l_1 + l_2 \\ l_1 \end{pmatrix} \hat{Q}^A_{l_1k_1} \hat{Q}^B_{l_2k_2} \times S^{k_1k_2}_{l_1l_2l_1+l_2} |\vec{X} - \vec{Y}|^{-l_1-l_2-1} \tag{9.15}$$

These moments, $\hat{Q}^A_{lm} = \int \mathrm{d}^3x \rho_A(\vec{x}) R_{lm}(\vec{x})$, interact with each other *via* a tensor that contains the distance and orientation dependence. Note that here we have used the fact that $|\vec{x} - \vec{y}| < |\vec{X} - \vec{Y}|$, namely, that the molecular charge densities must not interpenetrate. $R_{l,m}$, $I_{l,m}$ are the regular and irregular spherical harmonics, respectively.[148]

The molecular multipole moments can be converted between two coordinate frames, Σ_1 and Σ_2, according to:

$$Q^{(\Sigma_1)}_{lk} = \sum\nolimits_m Q^{(\Sigma_2)}_{lm} D^l_{mk}(\varphi, \theta, \psi)$$

Here, ϕ, θ, ψ are the Euler angles, and $[D^l_{mk}]$ is a Wigner rotation matrix. This allows one to perform the electrostatic parametrization of a molecule in a conveniently chosen local frame as well as include the transformation from the local to the global interaction frame in a tensor that takes care of both the distance and orientation dependence:

$$T^{A,B}_{l_1k_1l_2k_2} = \frac{1}{4\pi\varepsilon_0} \begin{pmatrix} l_1 + l_2 \\ l_1 \end{pmatrix} S^{k_1k_2}_{l_1l_2l_1+l_2} |\vec{X} - \vec{Y}|^{-l_1-l_2-1} \tag{9.16}$$

The interaction energy thus reduces to an expression consisting of only molecular multipole moments defined with respect to the molecular local frame and the generic interaction tensors $T^{A,B}_{l_1k_1l_2k_2}$ (tabulated up to $l_1 + l_3 = 5$ in ref. 149):

$$U_{AB} = \hat{Q}^A_{l_1k_1} T^{A,B}_{l_1k_1l_2k_2} \hat{Q}^B_{l_2k_2} \tag{9.17}$$

where we have used the Einstein sum convention for the multipole-moment components l_ik_i. The electrostatic part of the site-energy, which enters exponentially in the Marcus rate expression for a charge localized on molecule A, then reads:

$$\Delta U^{cn}_A = \sum_{B \neq A} (\hat{Q}^{A,c}_{l_1k_1} - \hat{Q}^{A,n}_{l_1k_1}) T^{A,B}_{l_1k_1l_2k_2} \hat{Q}^{B,n}_{l_2k_2} \tag{9.18}$$

where the superscripts c and n denote the molecular multipole moments in the neutral and charged state, respectively, and the sum extends over all external molecules B.

9.3.5.2 Distributed Multipoles

In eq. (9.17), we have provided an expression for the electrostatic interaction energy in terms of *molecule-centered* multipole moments. To arrive at this

expression, the separation between the molecular centers, $|\vec{X}-\vec{Y}|$, was assumed to be larger than that of any of the respective charge-carrying volume elements of the two molecules, $|\vec{x}-\vec{y}|$. In a molecular solid, this demand can hardly be satisfied, considering the dense packing and strongly anisotropic charge density. This inevitably leads to the breakdown of the single-point expansion at small separations. It is possible to avoid this breakdown by choosing multiple expansion sites per molecule in such a way as to accurately represent the molecular electrostatic potential, with a set of suitably chosen multipole moments $\{Q_{lk}^a\}$ allocated to each site. We then simply extend the expression for the interaction energy between two molecules A and B in the single-point expansion, eq. (9.17), and include the sum over all expansion sites $a \in A$ and $b \in B$:

$$U_{AB} = \sum_{a\in A}\sum_{b\in B} \hat{Q}^a_{l_1k_1} T^{a,b}_{l_1k_1l_2k_2} \hat{Q}^b_{l_2k_2} \equiv \hat{Q}^a_{l_1k_1} T^{a,b}_{l_1k_1l_2k_2} \hat{Q}^b_{l_2k_2} \tag{9.19}$$

Here, we have used the Einstein sum convention for the site indices a and b on the right-hand side of the equation, in addition to the same sum convention which is already in place for the multipole-moment components.

There are several strategies on how to arrive at such a collection of *distributed multipoles*,[14,15,150–153] which can be classified according to whether the multipoles are derived from the electrostatic potential, generated by the SCF charge density, or from a decomposition of the wavefunction itself. The CHELPG (CHarges from ELectrostatic Potentials, Grid-based) method, for example, relies on performing a least-squares fit of atom-placed charges to reproduce the electrostatic potential, as evaluated from the SCF density on a regularly spaced grid,[151,154] while the distributed multipole analysis (DMA)[152,153] operates directly on the quantum-mechanical density matrix, expanded in terms of atom- and bond-centered Gaussian functions.

9.3.5.3 Induction Interaction

Similar to the distributed multipole expansion of molecular electrostatic fields, one can derive a distributed polarizability expansion of the molecular field response by including the multipole-expansion in the perturbing Hamiltonian term $\hat{W} = \hat{Q}^a_t \phi^a_t$, where the Einstein sum convention is used for both superscripts a (referencing an expansion site) and subscripts t (summarizing the multipole components $(l,\ k)$ in a single index). Thus, the second-order energy correction reads[14]:

$$W^{(2)} = -\sum_{n\neq 0} \frac{|\langle 0|\hat{Q}^a_t \varphi^a_t|n\rangle|^2}{W_n - W_0} \tag{9.20}$$

We then absorb the quantum-mechanical response into a set of intramolecular site-site polarizabilites, where $-\alpha^{aa'}_{tt'}\phi^{a'}_{t'}$ yields the induced

multipole moment Q_t^a at site a, which results from a field component $\phi_{t'}^{a'}$ at site a'[14]:

$$\alpha_{tt'}^{aa'} = \sum_{n\neq 0} \frac{\langle 0|\hat{Q}_t^a|n\rangle\langle n|\hat{Q}_{t'}^{a'}|0\rangle}{W_n - W_0} + h.c. \tag{9.21}$$

With this set of higher-order polarizabilities at hand, we obtain the induction stabilization in a distributed formulation as $W^{(2)} = -\frac{1}{2}\varphi_t^a \alpha_{tt'}^{aa'} \varphi_{t'}^{a'}$. The derivatives of $W^{(2)}$ with respect to the components of the field ϕ_t^a at a polar site a then yield the correction to the permanent multipole moment Q_t^a at that site, $\Delta Q_t^a = \partial W^{(2)}/\partial \phi_t^a = -\alpha_{tt'}^{aa'} \phi_{t'}^{a'}$.

Using the multipole corrections ΔQ_t^a, we can now extend the electrostatic interaction energy (eq. 9.19) to include the induction contribution to the field energy U_{ext}, while accounting for the induction work U_{int}:

$$U_{\text{ext}} = \frac{1}{2}\sum_A \sum_{B\neq A} (Q_t^a + \Delta Q_t^a) T_{tu}^{ab} (Q_u^b + \Delta Q_u^b) \tag{9.22}$$

$$U_{\text{int}} = \frac{1}{2}\sum_A \Delta Q_t^a \eta_{tt'}^{aa'} \Delta Q_{t'}^{a'} \tag{9.23}$$

Here, the inverse of the positive-definite tensor $\eta_{tt'}^{aa'}$ is simply given by the distributed polarizabilities tensor $\alpha_{tt'}^{aa'}$, where we have included explicit sums over all molecules A and B.

We then use a variational approach to calculate the multipole corrections ΔQ_t^a:

$$\delta(U_{\text{ext}} + U_{\text{int}}) = \delta Q_t^a \left[\sum_{B\neq A} T_{tu}^{ab} (Q_u^b + \Delta Q_u^b) + \eta_{tt'}^{aa'} \Delta Q_{t'}^{a'} \right] \tag{9.24}$$

which leads to a set of self-consistent equations for the induced moments, which for large systems are solved iteratively:

$$\Delta Q_t^a = -\sum_{B\neq A} \alpha_{tt'}^{aa'} T_{t'u}^{a'b} (Q_u^b + \Delta Q_u^b) \tag{9.25}$$

The total energy can now be decomposed into two energy terms:

$$\begin{aligned} U_{pp} &= \sum_A \sum_{B>A} Q_t^a T_{tu}^{ab} Q_u^b \\ U_{pu} &= \frac{1}{2}\sum_A \sum_{B>A} \left[\Delta Q_t^a T_{tu}^{ab} Q_u^b + \Delta Q_t^b T_{tu}^{ab} Q_u^a \right] \end{aligned} \tag{9.26}$$

Here, $U_{pp} \leftrightarrow W^{(1)}$ is the electrostatic interaction energy, that is, the first-order correction due to the interaction of the permanent multipole moments. $U_{pu} \leftrightarrow W^{(2)}$ is the induction energy associated with the interaction of the

induced moments on a single molecule with the permanent moments induced on surrounding molecules.

9.3.5.4 Thole's Model

Equations (9.25) and (9.26) allow us to compute the electrostatic and induction energy contributions to the site energies in a self-consistent manner based on a set of molecular distributed multipoles $\{Q_t^a\}$ and polarizabilities $\{\alpha_{tt'}^{aa'}\}$, which can be obtained from wavefunction decomposition or fitting schemes, as discussed in Section 9.3.5.2. The $\{\alpha_{tt'}^{aa'}\}$ are formally given by eq. (9.21). This expression is somewhat impractical, though possible to evaluate (see ref. 152), such that various empirical methods have been developed. The Thole model,[155,156] for example, treats polarizabilities α^a in the local dipole approximation. It is based on a modified dipole–dipole interaction, which can be reformulated in terms of the interactions of smeared charge densities. This eliminates the divergence of the head-to-tail dipole–dipole interaction at small separations (Å scale).[155–157] Smearing out the charge distribution mimics the nature of the QM wavefunction, which effectively prevents the polarization catastrophe.

The smearing of the nuclei-centered multipole moments is obtained *via* a fractional charge density $\rho_f(\vec{u})$, which should be normalized to unity and fall off rapidly as of a certain radius $\vec{u} = \vec{u}(\vec{R})$. The latter is related to the physical distance vector $\vec{R}$, connecting two interacting sites *via* a linear scaling factor that takes into account the magnitude of the isotropic site polarizabilities α^a. This isotropic fractional charge density gives rise to a modified potential:

$$\varphi(u) = -\frac{1}{4\pi\varepsilon_0}\int_0^u 4\pi u'\rho(u')\mathrm{d}u' \tag{9.27}$$

The multipole interaction tensor $T_{ij\ldots}$ (this time in Cartesian coordinates) can be related to the fractional charge density in two steps: First, it is rewritten in terms of the scaled distance vector $\vec{u}$:

$$T_{ij\ldots}(\vec{R}) = f(\alpha^a\alpha^b)\, t_{ij\ldots}\left[\vec{u}(\vec{R}, \alpha^a\alpha^b)\right] \tag{9.28}$$

where the specific form of $f(\alpha^a\alpha^b)$ results from the choice of $u(\vec{R},\alpha^a\alpha^b)$. Second, the smeared interaction tensor $t_{ij\ldots}$ is given by the appropriate derivative of the potential in eq. (9.27):

$$t_{ij\ldots}(\vec{u}) = -\partial_{u_i}\partial_{u_j}\ldots\varphi(\vec{u}) \tag{9.29}$$

It turns out that for a suitable choice of $\rho_f(\vec{u})$, the modified interaction tensors can be rewritten in such a way that powers n of the distance $R = |\vec{R}|$ are damped *via* a damping function $\lambda_n\left[\vec{u}(\vec{R})\right]$.[158]

Several fractional charge densities $\rho_f(\vec{u})$ have been tested for the purpose of yielding best results for the molecular polarizability as well as the interaction energies. For most organic molecules, a fixed set of atomic polarizabilities

($\alpha_C = 1.334$, $\alpha_H = 0.496$, $\alpha_N = 1.073$, $\alpha_O = 0.873$, $\alpha_S = 2.926$ Å^3) based on atomic elements gives satisfactory results,[156] though reparametrizations are advised for ions and molecules with extended conjugated π-systems.

One of the common approaches, *e.g.*, in the AMOEBA force-field,[158] uses an exponentially-decaying fractional charge density:

$$\rho(u) = \frac{3a}{4\pi}\exp(-au^3) \tag{9.30}$$

where $\vec{u}(\vec{R}, \alpha^a\alpha^b) = \vec{R}/(\alpha^a\alpha^b)^{1/6}$ and $a = 0.39$ is the smearing exponent. The distance at which the charge–dipole interaction is reduced by a factor γ is then given by:

$$R_\gamma = \left[\frac{1}{a}\ln\left(\frac{1}{1-\gamma}\right)\right]^{1/3}(\alpha_i\alpha_j)^{1/6} \tag{9.31}$$

The interaction damping radius, associated with $\gamma = \frac{1}{2}$, revolves around an interaction distance of 2 Å. A half-interaction distance on this range indicates how damping is primarily important for the intramolecular field interaction of induced dipoles.

9.3.5.5 Case Studies

The expansion of the molecular field and field response in terms of distributed multipoles and polarizabilities is an efficient approach to solve for the first- and second-order corrections to the molecular Hamiltonian, which result from a perturbation by the molecular environment. This approach has been used to evaluate energetic landscapes in amorphous organic semiconductors,[47,51,52,159] where the width of the site energy distribution is often very large and can be attributed to randomly oriented molecular dipoles.[160,161] Owing to long-range electrostatic interactions, the resulting energetic disorder is always spatially correlated (Figure 9.7a). Spatial correlations lead to current filaments, as shown in Figure 9.7(a,b), and a Poole–Frenkel dependence of the charge carrier mobility on the externally applied electric field.[162]

Using this perturbative approach, it has also been shown that thermal fluctuations can lead to large variations in local electric fields and, hence, large energetic disorder (even in crystalline systems).[44,144,147] Finally, the method has also been employed to study energetics at organic interfaces.[49,163–169] Additional complications associated with the dimensionality reduction at interfaces and long-ranginess of Coulomb interactions are discussed in Section 9.6.

For crystalline polymers, it has been shown that the width of the distribution of the site energies (energetic disorder) depends on the side-chain packing and polymer regioregularity: 100% regioregular P3HT always has narrower site energy distributions than the 90% P3HT,[44,144] The magnitude of the disorder compares well with the width of the DOS, as extracted from

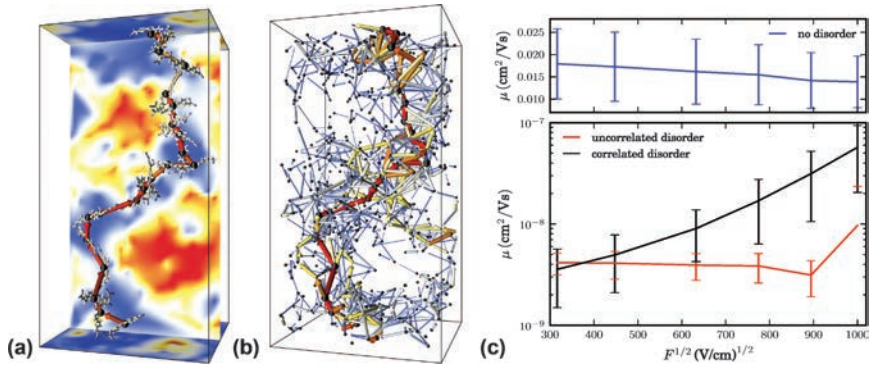

Figure 9.7 (a) Current filament and energetic landscape visualized in a slice of a disordered (amorphous) morphology of DCV4T. (b) Local currents contributing to 90% of the total current in the system. The dots are the molecular centers of mass, while the arrows depict the local currents (their thickness and color are proportional to the logarithm of the current's amplitude). Adapted with permission from ref. 159. Copyright (2012) The Royal Society of Chemistry. (c) Poole–Frenkel plots for a system of 4096 Alq_3 molecules. To illustrate the role of disorder and correlations, we show the field dependence for a system without energetic disorder (top panel) and without spatial correlations, that is after randomly shuffling site energies.
Adapted with permission from ref. 140. Copyright (2011) The American Chemical Society.

time-of-flight experiments,[170,171] where values for σ of 56 and 71 meV, respectively, have been proposed from a fit of the field-dependence of the mobility as obtained within the Gaussian disorder model.[8] On the level of chain ordering, the increase in energetic disorder can also be related to the increase in paracrystallinity along the π-stacking direction,[44] with the energetic disorder being linearly related to the amplitude of backbone–backbone distance fluctuations.

9.3.6 Charge Mobility

With the site energies and electronic couplings at hand, one is now able to calculate charge transfer rates (Section 9.3.2) for the set of electronically coupled pairs of conjugated segments. The directed graph which describes charge transport in the system is then fully parametrized and charge dynamics can be described *via* a master equation of the form:

$$\frac{\partial P_\alpha}{\partial t} = \sum_\beta \left[P_\beta K_{\beta\to\alpha} - P_\alpha K_{\alpha\to\beta} \right] \tag{9.32}$$

where P_α is the probability to find the systems in state α. The rates $K_{\alpha\to\beta}$ are the transition rates from state α to state β. For single-carrier dynamics, the number of available states α is the number of conjugated segments in the

system, with each state associated with molecule A being singly occupied. Using the single-site occupation probability P_A and transfer rates $K_{A\to B}$, eq. (9.32) simplifies to:

$$\frac{\partial p_A}{\partial t} = \sum_B [p_B k_{B\to A} - p_A k_{A\to B}] \tag{9.33}$$

This equation, valid in the limit of low charge densities, has the form $\partial_t \vec{p} = \tilde{k}\vec{p}$ and can be solved using linear solvers. In the more general cases (*i.e.* more than one carrier), expressing eq. (9.32) in terms of site occupation probabilities can be done using a mean-field approximation.[172] For this, the analogue of eq. (9.33) becomes, however, nonlinear and requires special solvers. If, in addition, several different types of carriers (holes, electrons, excitons) are present in the system, with their creation/annihilation processes taking place, it is practically impossible to link state and site occupation probabilities to the corresponding rates.

Instead, the solution of eq. (9.32) can be obtained by means of kinetic Monte Carlo (KMC) methods. KMC explicitly simulates the dynamics of charge carriers by constructing a Markov chain in state space and is suitable for both transient and stationary solutions of the master equation. A variable time-step size implementation of KMC is often employed due to the broad distribution of rates $K_{A\to B}$, which easily spans many orders of magnitude.

The stationary solution of eq. (9.33) can be used to evaluate several macroscopic observables.[47] For comparison with TOF, impedance spectroscopy, or similar measurements, the charge-carrier mobility tensor $\tilde{\mu}$ in the electric field $\vec{E}$ can be calculated as:

$$\tilde{\mu}\vec{E} = \sum_{A,B} p_A k_{A\to B}(\vec{R}_A - \vec{R}_B) \tag{9.34}$$

Alternatively, the charge-carrier mobility along the direction of the external field $\vec{E}$ can be obtained from a trajectory:

$$\mu = < \frac{\Delta\vec{R}\cdot\vec{E}}{\Delta t|\vec{E}|^2} > \tag{9.35}$$

where $<\ldots>$ denotes averaging over all trajectories, Δt is the total run time of a trajectory and $\Delta\vec{R}$ denotes the net displacement of the charge.

Charge dynamics are therefore guided by an interplay of topological connectivity of the directed graph, determined by the electronic coupling elements, and the ratios of forward to backward rates, prescribed by the energetic landscape. In discotic liquid crystals, for example, the graph is practically one-dimensional, *i.e.* even a few defects can block charge transport along π-conjugated columns.[143,173,174] In crystalline organic semiconductors, the presence of a strong well-defined π-stacking direction can turn out to be disadvantageous for efficient charge transport, since it might inhibit other transport directions and is prone to charge trapping if energetic disorder is present in the system.[147,159] In amorphous

semiconductors, the directed graph is always three-dimensional and the transport is mostly determined by energetic disorder and correlations, as illustrated in Figure 9.7(c) for a system of 4096 Alq_3 molecules. Here, the energetic disorder reduces the value of mobility by six orders of magnitude. The Poole–Frenkel behavior for small fields can only be observed if correlated disorder is taken into account. Note that for systems with large energetic disorder, simulations systematically overestimate the absolute values of non-dispersive mobilities due to significant finite size effects (see also Section 9.4).

Transport studies on different levels of complexity have been performed to investigate hole transport along the π-stacking direction of conjugated polymers.[36,44,144,175] Since the transport has a one-dimensional character, it can already be anticipated that a broad distribution of electronic couplings limits the charge mobility along the lamellae.[147,159,173,174,176–179] Indeed, mobility values are typically broadly distributed (from lamellae to lamelae), with small mobilities as low as 10^{-7} cm^2 V^{-1} s^{-1} for P3HT.[44] It has also been observed that the regioregularity effect occurs exclusively due to increased energetic disorder and that the higher mobility in the more regioregular material is entirely attributable to the narrowing of the density of states that arises from an increased order in hole–quadrupole interaction distances. This reduction can be traced back to the amplified fluctuations in backbone–backbone distances, *i.e.* the material's paracrystallinity.

9.4 Finite-Size Effects

Microscopic charge transport simulations are computationally demanding: First, electronic coupling elements need to be evaluated for all neighboring molecules. Second, evaluation of the electrostatic and induction contributions to the site energy requires large cutoffs or even special summation techniques (Section 9.6). This sets the limit on system sizes, which currently is on the order of hundreds of thousands of molecules. It is thus important to make sure that there are no finite size effects present when evaluating macroscopic properties of the system.

In fact, these effects are observed even experimentally in systems with large energetic disorder. Indeed, time-of-flight measurements of mobility can become unreliable: in thin organic films charge transport is dispersive and transients do not have a characteristic plateau used to determine the transient time.[6,180–182] Using thicker samples normally remedies the situation. It might seem that one can perform the same trick in computer simulations and replicate the (periodic) simulation box in the direction of the applied field. It turns out that the straightforward increase in the system size will still give incorrect (higher) values of charge carrier mobility. The reason for this is that all duplicated boxes have exactly the same (and small) number of independent site energies. Hence, statistical averages will always be performed over this small set of site energies, and charge carriers will traverse the sample at a different (higher) temperature than in an infinitely

large system. An additional averaging over different (statistically uncorrelated) repeated snapshots is required, since the origin of the problem is in the limited number of sites available for every distinct Monte Carlo simulation.

This type of finite size effects becomes much smaller at higher temperatures, since the relevant dimensionless parameter (at least in the Gaussian disorder model) is the width of the site energy distribution σ divided by k_BT. In fact, an empirical expression:

$$(\sigma/k_BT_{ND})^2 = -5.7 + 1.05 \ln N$$

can be used to estimate at what temperature the ''transition'' between the dispersive and non-dispersive transport occurs, where N is the number of the hopping sites (molecules) in the system. This observation has been used to perform an *ad hoc* correction of finite-size effects[183]: Nondispersive mobilities were calculated for a set of temperatures above T_{ND}. Then, an explicit temperature dependence was used to extrapolate the value of mobility to room temperature.

A clear drawback of this method is that is relies on an explicit knowledge of the temperature-dependence of mobility. While the exact analytical expression of this dependence is available only for one-dimensional systems[184,185]:

$$\mu(T) = \frac{\mu_0}{T^{3/2}} \exp\left[-\left(\frac{a}{T}\right)^2 - \left(\frac{b}{T}\right)\right] \tag{9.36}$$

it can still be used in a three-dimensional case in a rather broad temperature range (this has been verified by performing simulations for systems of different sizes and at different temperatures).

To illustrate the relevance of such extrapolation, charge transport in the amorphous mesophase of Alq_3 has been simulated in systems of different sizes.[183] In a system of 512 molecules simulated mobility was of the order of 10^{-6} cm^2 V^{-1} s^{-1}, while in a box of 4096 molecules an order of magnitude lower value has been measured. An extrapolation procedure resulted in a mobility of 10^{-9} cm^2 V^{-1} s^{-1}, which is three orders of magnitude lower than the one simulated in a small system. Note that the magnitude of the correction is very sensitive to the value of energetic disorder σ. While in Alq_3 $\sigma = 0.14$ eV, in an amorphous DCV4T $\sigma = 0.25$ eV and one can overestimate the value of mobility by seven(!) orders of magnitude.[186]

9.5 Stochastic Models

A separate issue of organic materials is their stability. This is especially important for OLEDs, where the efficiency roll-off and life-time of a device are intimately connected. Device degradation modeling poses, however, statistical challenges, since we are dealing with rare events that require large

simulation boxes, in particular in the lateral dimension (which in OLED is of the order of square mm). A pragmatic solution to this problem is to parametrize a mesoscopic lattice model (*e.g.* Gaussian disorder model, GDM) on the results of microscopic simulations and use this model to study charge/exciton distributions and dynamics in larger systems.[186]

The convenience of GDM originates from their simplicity: material morphology is represented by a regular lattice, while charge transfer rates decay exponentially with the intermolecular separation and energy differences are incorporated *via* the Boltzmann prefactor. This approach, initiated by Bässler, has been successfully used by several groups to understand the role of traps, finite charge carrier density, energetic disorder, and other mesoscopic parameters on charge mobility.[8,13,161,187–190]

At the same time, the necessity of extending the existing discrete mesoscopic models has also become clear: first, the parametrization based on microscopic simulations is not straightforward.[186] Second, either stationary or transient quantities are quantitatively reproduced, while for the description of transient (degradation) processes both should agree with experimental data. A potential solution to this problem is to introduce an off-lattice model, which can be directly linked to the microscopic model and would thus offer a much closer description of physical processes in the system.

One of the ways to achieve this is to provide a stochastic way of generating the material morphology and charge transfer rates.[191–193] For morphologies, for example, a stochastic process should reproduce given correlation functions, densities, and coordination numbers. For the charge transfer rates, a simple procedure can be developed by analyzing the distributions of parameters entering the charge transfer rate. In an amorphous mesophase of Alq_3, for example, the distribution of electronic couplings at every particular intermolecular separation is Gaussian. The dependence of the width and the mean of this Gaussian on intermolecular separation can be determined from microscopic simulations. Regarding the site energies, spatial correlations can be introduced by using a moving-average procedure, where site energies of the neighbors within a certain cutoff are mixed into initially independent Gaussian site-energy distribution.

Stochastic models developed for amorphous mesophases of Alq_3 and DCV4T could reproduce the mobility-field and mobility-density dependencies.[186,191,193] This indicates that they indeed can serve as an intermediate step between the completely microscopic descriptions and macroscopic, drift-diffusion-equations based models. The current challenge is to extend such models to anisotropic and heterogeneous systems.

9.6 Interfaces and Long-Range Interactions

As discussed in Section 9.3.5, the contribution of the environment to the energy of a localized charged state is taken into account in a perturbative

way, by evaluating the corresponding electrostatic and induction terms. Van der Waals interactions are normally ignored, since only the site energy differences enter the charge transfer rate, *i.e.* if the molecular polarization tensor does not change upon charging a molecule, this contribution is negligible. Evaluation of the electrostatic contribution includes, among others, Coulomb interactions of partial charges or higher distributed multipoles. These interactions are inherently long-range and require special summation techniques, *e.g.* Ewald summation, which is widely used in atomistic molecular dynamics simulations.[194] In this approach, the Coulomb interaction potential is split into two terms, one of which is converging rapidly in real and the other in reciprocal space. Induction contribution can also be incorporated in such a scheme.[158] While this method is well developed, it is designed for neutral systems, whereas for charge transport we would be interested in energies of a localized charge interacting with the neutral environment. The presence of a charged excitation (and its polarization cloud) violates periodicity of the system, which is essential for calculations in the reciprocal space.

A solution to this problem has been proposed by Poelking *et al.*[195]: the non-periodic (foreground) part of the system, which incorporates the charged excitation and its induction cloud, is superimposed onto a periodic, neutral background, which is computed using the Ewald summation method. The real-space interaction between these two regions is mediated by fields created by the background charge distribution, including induced moments. A modified shape term[196] is added to account for the net charge and quadrupole of the simulations cell. This term takes into account surface effects and depends on the summation geometry.

By applying this technique to organic/organic interfaces it has been shown that a cutoff of 4–8 nm is sufficient to converge the energy of a periodic three-dimensional system. For heterogeneous ordered systems (*e.g.* interfaces) the convergence turns out to be significantly slower, for example for a 12 nm thick slab the energy is far from converged even for the cutoff of 22 nm (see ref. 195 and Figure 9.8). Hence, this method is imperative to use in two-dimensional periodic systems or, in general, heterogeneous systems with a long-range molecular ordering. The differences between using simulations with a cutoff and without it are remarkable: the additional electrostatic/induction contribution can change from 0.5 eV (10 nm cutoff) to –0.7 eV (infinite system). The correct treatment of electrostatic contribution can therefore *reverse* the role of donor and acceptor as conditioned by gas-phase energy levels and energy levels calculated with a seemingly ample cutoff. It also predicts that the energy profiles for electrons and holes are flat at the organic–organic interfaces, while cutoff based calculations lead to a significant level bending. Finally, it allows to establish a relationship between structural coherence and state energetics: the structural coherence is probed up to a μm scale, hence emphasizing the role of extended crystallites (and their alignment) at interfaces.

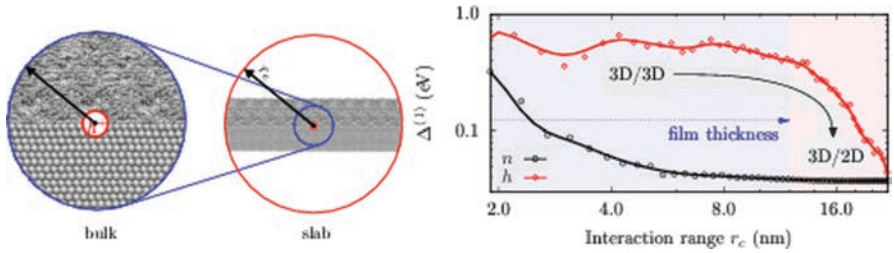

Figure 9.8 Variation of the electrostatic interaction energy with interaction range (r_c) for a positively charged (h) and neutral (n) DCV4T molecule in a nematically ordered thin film of thickness 12 nm. The crossover from a bulk-like to a slab-like convergence occurs as r_c exceeds film thickness. The converged value for a positively charge molecule is –0.7 eV (not shown on the graph).

9.7 Excited States

Excited and charge transfer states are at the heart of the functionality of solar cells and OLEDs. Through them, photons dissociate into free charges and free charges recombine radiatively. In both situations, however, processes related to these excitations are still poorly understood. Efficient exciton dissociation, for example, has been attributed to the assistance of charge separation by a gradient in the free-energy landscape,[197,198] structural heterogeneity as a function of distance to the interface,[199] doping and charged defects,[200] increase in entropy as the electron and hole move away from the interface,[201] formation of hot charge transfer states,[202] or long-range tunneling.[203] To gain more microscopic insight into the role of excited and charge transfer states is not only of fundamental interest, but is also directly relevant for a better understanding of, for example, the shape of the current–voltage curves of photovoltaic devices. For solar cells, in particular, this should help to understand the origin of the fill factor, which largely determines the device efficiency and can vary dramatically between different blends.

We therefore must aim at quantitative descriptions of excited states, their rates of geminate and non-geminate recombination, mobilities and diffusion coefficients. Such quantitative studies, however, require an accurate description of nonlocal electron–hole interactions. To this end, there is no optimal method for taking them into account and the scientific community has attempted various approaches. Among the available methods, the use of time-dependent density-functional theory (TDDFT)[204] is appealing because of its moderate computational demands. TDDFT calculations based on local exchange-correlation kernels yield reasonable excitation energies for small- and medium-sized molecules, provided that the excited states are formed from local transitions, are mainly composed of a single transition, and no extended π-systems are involved.[205,206]

Such assumptions are, however, problematic for charge-transfer excitons,[207,208] for which the interactions of spatially separated electrons (on acceptor) and holes (on donor) are not correctly described. Range-separated exchange-correlation kernels[209,210] can be used to overcome this deficiency but often need compound-specific adjustments.[211,212] Quantum-chemical approaches, such as coupled-cluster methods, on the other hand, allow for an accurate treatment of electron–electron and electron–hole interactions, but are computationally too demanding.[213–215]

Recently, it has been shown that the limitations of these methods can be overcome by using many-body Green's functions theory within the GW approximation and the Bethe–Salpeter equation (GW-BSE).[216–218] It has been successfully applied to determine optical excitations in crystals,[219–221] polymers,[222,223] and small inorganic[224,225] and organic[223,226] molecules.

To this end, the many-body Green's functions theory within the GW approximation and the Bethe–Salpeter equation have been benchmarked for a series of prototypical small-molecule based pairs.[227–229] This method has predicted energies of local Frenkel and intermolecular charge-transfer excitations with an accuracy of tens of meV.[230] Analysis of energy levels and binding energies of excitons in dimers of dicyanovinyl-substituted quaterthiophene and fullerene[231] as well as zinc-tetraphenylporphyrin and C_{70}-fullerene[232] has shown that the transition from Frenkel to charge transfer excitons is endothermic and the binding energy of charge transfer excitons is still of the order of 1.5–2 eV. Hence, even such an accurate dimer-in-vacuum-based description does not yield internal energetics favorable for the generation of free charges either by thermal energy or by an external electric field. These results indicate that accounting for the explicit molecular environment is as important as an accurate knowledge of internal dimer energies and should clearly be the focus of research aiming at quantitative descriptions of excitations in organic materials.

9.8 Software

An extensive list of standard simulations packages can be found elsewhere.[48,233] Here, we only provide a brief overview of the package that was especially designed for coarse-grained simulations of morphologies and microscopic calculations of charge mobility, the Versatile Object-oriented Toolkit for Coarse-graining and Charge Transport Applications (VOTCA, www.votca.org). Most of the aforementioned methods are implemented in this package (Figure 9.9).

VOTCA consists of several modules: systematic coarse-graining (VOTCA-CSG), charge/exciton transport (VOTCA-CTP, VOTCA-MOO), and the kinetic Monte Carlo (VOTCA-KMC). The coarse-graining (VOTCA-CSG) package[55] implements several coarse-graining techniques, among them force-matching, inverse Monte Carlo, and iterative Boltzmann inversion. It is a platform for method development of new approaches for obtaining well-defined coarse-grained models. The purpose of the charge transport (VOTCA-CTP)

package[140] is to simplify the work-flow for charge and energy transport simulations, provide a uniform error control for these methods, a flexible platform for their development, and to eventually also allow for *in silico* pre-screening of organic semiconductors for specific applications.

A typical work-flow of charge transport simulations is depicted in Figure 9.9. The first step is the simulation of the atomistic morphology (VOTCA-CSG), which is then partitioned into hopping sites. Subsequently, the coordinates of the hopping sites are used to construct a list of pairs of molecules, known as the neighbor list. For each pair, an electronic coupling element (VOTCA-MOO), the reorganization energy, the driving force, and eventually the hopping rate are evaluated. The neighbor list, combined with the hopping rates, defines a directed graph. The corresponding master equation can then be solved using the kinetic Monte Carlo method (VOTCA-KMC), which allows one to explicitly monitor the charge dynamics in a system, as well as calculate time- or ensemble-averages of occupation probabilities, charge fluxes, correlation functions, and field-dependent mobilities.

The package is written in modular C++ while the workflow is implemented using scripting languages and controlled by several extensible

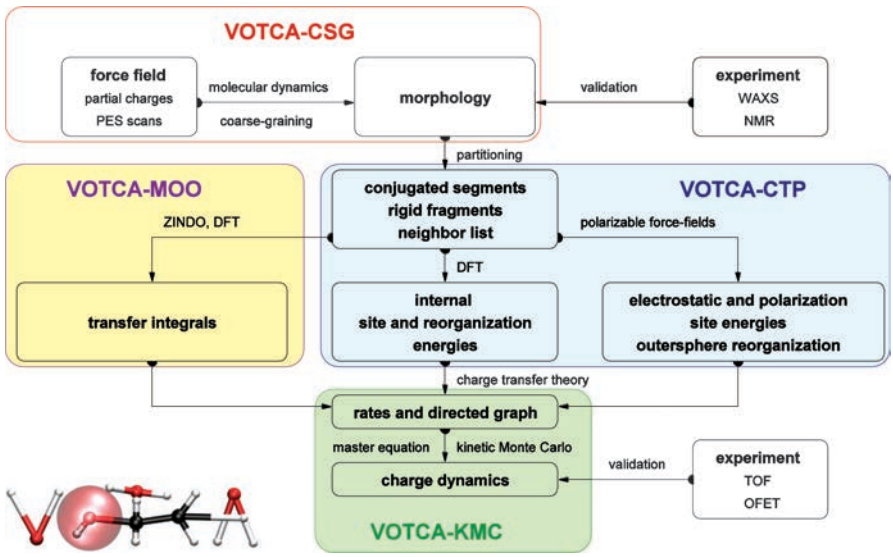

Figure 9.9 Modules of the VOTCA package, www.votca.org: Ground-state geometries, partial charges, refined force-fields, and coarse-grained models are used to simulate atomistically-resolved morphologies. After partitioning on conjugated segments and rigid fragments, a list of pairs of molecules (neighbor list) can be constructed. Transfer integrals, reorganization and site energies, and eventually hopping rates are then calculated for all pairs from this list. From this, a directed graph is generated and the corresponding master equation is solved using the kinetic Monte Carlo method.

markup language (XML) input files, which make it a robust yet easily modifiable toolkit for new developers. The code is available as a complete package in various Linux distributions and is partitioned into five libraries (tools, csg, ctp, kmc, moo), with each library providing a distinct functionality. Data transfer between individual programs is implemented *via* a relational (SQLite) database. CMake is used to build, test, and package the toolkit.

9.9 Outlook

To conclude, substantial method development is still necessary to achieve parameter-free modeling of organic semiconductors. Although the list is far from complete, several methodological issues to resolve are:

- Prediction of partially-ordered, non-equilibrium morphologies influenced by the material's processing, especially for polymeric semiconductors. This includes force-field parametrization from first-principles and the development of accurate coarse-grained models, as well as advanced sampling techniques.
- Definition of diabatic states, in particular if they are delocalized over parts of the molecule or over several molecules.
- Development of more accurate and efficient methods for the evaluation of electrostatic and induction effects when evaluating site energy differences, especially for charged systems with aperiodic charge distributions in a periodic neutral environment.
- Embedding of (computationally demanding) treatment of explicit long-range Coulomb interactions (including induction) when solving the master equation, *i.e.* re-evaluation of state-dependent rates at every Monte Carlo step.
- Developing computationally efficient off-lattice models for morphologies and rates, as well as the parametrization techniques for specific compounds.
- Quantitative treatment of excited states embedded in a heterogeneous polarizable molecular environment.

Note, that advancements in all of the above-mentioned directions are absolutely vital before one can even start to think about devising accurate structure–property relationships for organic semiconductors.

Acknowledgements

This work was partly supported by the DFG program IRTG 1404, DFG grant SPP 1355, and BMBF grants MEDOS (FKZ 03EK3503B) and MESOMERIE (FKZ 13N10723). We are grateful to Carl Poelking, Pascal Kordt, Anton Melnyk, Jens Wehner, Kurt Kremer, and Mara Jochum for critical reading of this manuscript.

References

1. Wolfgang Tress, Karl Leo and Moritz Riede, Influence of hole-transport layers and donor materials on open-circuit voltage and shape of i-v curves of organic solar cells, *Adv. Funct. Mater.*, 2011, **21**(11), 2140–2149.
2. Thomas Kirchartz and Jenny Nelson, Device modelling of organic bulk heterojunction solar cells, *Top. Curr. Chem.*, 2013, 1–46.
3. P. de Bruyn, A. H. P. van Rest, G. a. H. Wetzelaer, D. M. de Leeuw and P. W. M. Blom, Diffusion-limited current in organic metal-insulator-metal diodes, *Phys. Rev. Lett.*, 2013, **111**(18), 186801.
4. L. J. A. Koster, V. D. Mihailetchi, R. Ramaker and P. W. M. Blom, Light intensity dependence of open-circuit voltage of polymer:fullerene solar cells, *Appl. Phys. Lett.*, 2005, **86**(12), 123509.
5. Ilja Lange, Juliane Kniepert, Patrick Pingel, Ines Dumsch, Sybille Allard, Silvia Janietz, Ullrich Scherf and Dieter Neher, Correlation between the open circuit voltage and the energetics of organic bulk heterojunction solar cells, *J. Phys. Chem. Lett.*, 2013, **4**(22), 3865–3871.
6. Harvey Scher and Elliott Montroll, Anomalous transit-time dispersion in amorphous solids, *Phys. Rev. B*, 1975, **12**(6), 2455–2477.
7. B. Movaghar, B. Pohlmann and W. Schirmacher, Theory of electronic hopping transport in disordered materials, *Philosophical Magazine Part B*, 1980, **41**(1), 49–63.
8. H. Baessler, Charge transport in disordered organic photoconductors a Monte Carlo simulation study, *Phys. Status Solidi B*, 1993, **175**(1), 15–56.
9. Sergei Baranovski and Oleg Rubel, Description of charge transport in amorphous semiconductors. In Sergei Baranovski, editor, *Charge Transport in Disordered Solids with Applications in Electronics*, pages 49–96. John Wiley & Sons, Ltd, 2006.
10. M. Bouhassoune, S. L. M. van Mensfoort, P. A. Bobbert and R. Coehoorn, Carrier-density and field-dependent charge-carrier mobility in organic semiconductors with correlated gaussian disorder, *Organic Electronics*, 2009, **10**(3), 437–445.
11. J. O. Oelerich, D. Huemmer, M. Weseloh and S. D. Baranovskii, Concentration dependence of the transport energy level for charge carriers in organic semiconductors, *Appl. Phys. Lett.*, 2010, **97**(14), 143302.
12. S. D. Baranovskii, Theoretical description of charge transport in disordered organic semiconductors, *Physica Status Solidi (b)*, 2014, **251**(3), 487–525.
13. W. F. Pasveer, J. Cottaar, C. Tanase, R. Coehoorn, P. A. Bobbert, P. W. M. Blom, D. M. de Leeuw and M. A. J. Michels, Unified description of charge-carrier mobilities in disordered semiconducting polymers, *Phys. Rev. Lett.*, 2005, **94**(20), 206601.
14. A. J Stone. *The Theory of Intermolecular Forces*. Clarendon Press, Oxford, 1997.

15. Christian Kramer, Tristan Bereau, Alexander Spinn, Klaus R. Liedl, Peter Gedeck and Markus Meuwly, Deriving static atomic multipoles from the electrostatic potential, *Journal of Chemical Information and Modeling*, 2013, **53**(12), 3410–3417.
16. Alexandre Tkatchenko, Robert A. DiStasio, Roberto Car and Matthias Scheffler, Accurate and efficient method for many-body van der Waals interactions, *Phys. Rev. Lett.*, 2012, **108**(23), 236402.
17. Pedro E. M. Lopes, Benoit Roux and Alexander D. MacKerell Jr, Molecular modeling and dynamics studies with explicit inclusion of electronic polarizability: theory and applications, *Theoretical Chemistry Accounts*, 2009, **124**(1–2), 11–28.
18. Piotr Cieplak, François-Yves Dupradeau, Yong Duan and Junmei Wang, Polarization effects in molecular mechanical force fields, *J. Phys-Condens. Mat.*, 2009, **21**(33), 333102.
19. Seiji Tsuzuki, Kazumasa Honda and Reiko Azumi, Model chemistry calculations of thiophene dimer interactions: Origin of -stacking, *J. Am. Chem. Soc.*, 2002, **124**(41), 12200–12209.
20. Seth B. Darling and Michael Sternberg, Importance of side chains and backbone length in defect modeling of poly(3-alkylthiophenes), *J. Phys. Chem. B*, 2009, **113**(18), 6215–6218.
21. C. F. N. Marchiori and M. Koehler, Dipole assisted exciton dissociation at conjugated polymer/fullerene photovoltaic interfaces: A molecular study using density functional theory calculations, *Synthetic Metals*, 2010, **160**(7–8), 643–650.
22. Ram S. Bhatta, Yeneneh Y. Yimer, Mesfin Tsige and David S. Perry, Conformations and torsional potentials of poly(3-hexylthiophene) oligomers: Density functional calculations up to the dodecamer, *Computational and Theoretical Chemistry*, 2012, **995**, 36–42.
23. Antonino Famulari, Guido Raos, Alberto Baggioli, Mosè Casalegno, Riccardo Po and Stefano V. Meille, A solid state density functional study of crystalline thiophene-based oligomers and polymers, *J. Phys. Chem. B*, 2012, **116**(49), 14504–14509.
24. Ram S. Bhatta, Yeneneh Y. Yimer, David S. Perry and Mesfin Tsige, Improved force field for molecular modeling of poly(3-hexylthiophene), *J. Phys. Chem. B*, 2013, **117**(34), 10035–10045.
25. Ram S. Bhatta and David S. Perry, Correlated backbone torsional potentials in poly(3-methylthiophene), *Computational and Theoretical Chemistry*, 2013, **1008**, 90–95.
26. Alberto Baggioli and Antonino Famulari, On the inter-ring torsion potential of regioregular p3ht: a first principles reexamination with explicit side chains, *Phys. Chem. Chem. Phys.*, 2014, **16**(9), 3983–3994.
27. Arnaud Maillard and Alain Rochefort, Structural and electronic properties of poly(3-hexylthiophene) π-stacked crystals, *Phys. Rev. B*, 2009, **79**(11).
28. Renato Colle, Giuseppe Grosso, Alberto Ronzani and Claudio M. Zicovich-Wilson, Structure and x-ray spectrum of crystalline poly(3-hexylthiophene)

from DFT-van der Waals calculations, *physica status solidi (b)*, 2011, **248**(6), 1360–1368.
29. Weiyu Xie, Y. Y. Sun, S. B. Zhang and John E. Northrup, Structure and sources of disorder in poly(3-hexylthiophene) crystals investigated by density functional calculations with van der Waals interactions, *Phys. Rev. B*, 2011, **83**(18), 184117.
30. Stefan Grimme, Semiempirical GGA-type density functional constructed with a long-range dispersion correction, *J. Comput. Chem.*, 2006, **27**(15), 1787–1799.
31. O. Anatole von Lilienfeld, Ivano Tavernelli, Ursula Rothlisberger and Daniel Sebastiani, Optimization of effective atom centered potentials for london dispersion forces in density functional theory, *Phys. Rev. Lett.*, 2004, **93**(15), 153004.
32. D. C. Langreth, B. I. Lundqvist, S. D. Chakarova-Käck, V. R. Cooper, M. Dion, P. Hyldgaard, A. Kelkkanen, J. Kleis, Lingzhu Kong, Shen Li, P. G. Moses, E. Murray, A. Puzder, H. Rydberg, E. Schröder and T. Thonhauser, A density functional for sparse matter, *J. Phys-Condens. Mat.*, 2009, **21**(8), 084203.
33. Oleg A. Vydrov and Troy Van Voorhis, Nonlocal van der Waals density functional made simple, *Phys. Rev. Lett.*, 2009, **103**(6), 063004.
34. K. Hannewald and P. A. Bobbert, Ab initio theory of charge-carrier conduction in ultrapure organic crystals, *Appl. Phys. Lett.*, 2004, **85**(9), 1535.
35. David L. Cheung and Alessandro Troisi, Modelling charge transport in organic semiconductors: from quantum dynamics to soft matter, *Phys. Chem. Chem. Phys.*, 2008, **10**(39), 5941.
36. David P. McMahon, David L. Cheung, Ludwig Goris, Javier Dacuna, Alberto Salleo and Alessandro Troisi, Relation between microstructure and charge transport in polymers of different regioregularity, *J. Phys. Chem. C*, 2011, **115**(39), 19386–19393.
37. Thorsten Vehoff, Yeon Sook Chung, Karen Johnston, Alessandro Troisi, Do Y. Yoon and Denis Andrienko, Charge transport in self-assembled semiconducting organic layers: Role of dynamic and static disorder, *J. Phys. Chem. C*, 2010, **114**(23), 10592–10597.
38. A. Troisi and G. Orlandi, Charge-transport regime of crystalline organic semiconductors: Diffusion limited by thermal off-diagonal electronic disorder, *Phys. Rev. Lett.*, 2006, **96**(8).
39. Frank Ortmann, Friedhelm Bechstedt and Karsten Hannewald, Charge transport in organic crystals: Theory and modelling, *Physica Status Solidi (b)*, 2011, **248**(3), 511–525.
40. A. D. MacKerell, D. Bashford, M. Bellott, R. L. Dunbrack, J. D. Evanseck, M. J. Field, S. Fischer, J. Gao, H. Guo, S. Ha, D. Joseph-McCarthy, L. Kuchnir, K. Kuczera, F. T. K. Lau, C. Mattos, S. Michnick, T. Ngo, D. T. Nguyen, B. Prodhom, W. E. Reiher, B. Roux, M. Schlenkrich, J. C. Smith, R. Stote, J. Straub, M. Watanabe, J. Wiórkiewicz-Kuczera, D. Yin and M. Karplus, All-atom empirical potential for molecular

modeling and dynamics studies of proteins, *J. Phys. Chem. B*, 1998, **102**(18), 3586–3616.
41. William L. Jorgensen, David S. Maxwell and Julian Tirado-Rives, Development and testing of the OPLS all-atom force field on conformational energetics and properties of organic liquids, *J. Am. Chem. Soc.*, 1996, **118**(45), 11225–11236.
42. Wendy D. Cornell, Piotr Cieplak, Christopher I. Bayly, Ian R. Gould, Kenneth M. Merz, David M. Ferguson, David C. Spellmeyer, Thomas Fox, James W. Caldwell and Peter A. Kollman, A second generation force field for the simulation of proteins, nucleic acids, and organic molecules, *J. Am. Chem. Soc.*, 1995, **117**(19), 5179–5197.
43. Valentina Marcon and Guido Raos, Molecular modeling of crystalline oligothiophenes: Testing and development of improved force fields, *J. Phys. Chem. B*, 2004, **108**(46), 18053–18064.
44. Carl Poelking and Denis Andrienko, Effect of polymorphism, regioregularity and paracrystallinity on charge transport in poly(3-hexylthiophene) p3ht. nanofibers, *Macromolecules*, 2013, **46**(22), 8941–8956.
45. Margherita Moreno, Mosè Casalegno, Guido Raos, Stefano V. Meille and Riccardo Po, Molecular modeling of crystalline alkylthiophene oligomers and polymers, *J. Phys. Chem. B*, 2010, **114**(4), 1591–1602.
46. Tran Thinh To and Stefan Adams, Accurate poly(3-hexylthiophene) forcefield from first-principle modeling, *Nanoscience and Nanotechnology Letters*, 2012, **4**(7), 703–711.
47. Victor Rühle, James Kirkpatrick and Denis Andrienko, A multiscale description of charge transport in conjugated oligomers, *J. Chem. Phys.*, 2010, **132**(13), 134103–134103–9.
48. Luca Muccioli, Gabriele D'Avino, Roberto Berardi, Silvia Orlandi, Antonio Pizzirusso, Matteo Ricci, Otello Maria Roscioni and Claudio Zannoni, Supramolecular organization of functional organic materials in the bulk and at organic/organic interfaces: A modeling and computer simulation approach, *Top. Curr. Chem.*, 2013, 1–63.
49. Gabriele D'Avino, Sébastien Mothy, Luca Muccioli, Claudio Zannoni, Linjun Wang, Jérôme Cornil, David Beljonne and Frédéric Castet, Energetics of electron–hole separation at p3ht/PCBM heterojunctions, *J. Phys. Chem. C*, 2013, **117**(25), 12981–12990.
50. Orestis Alexiadis and Vlasis G. Mavrantzas, All-atom molecular dynamics simulation of temperature effects on the structural, thermodynamic, and packing properties of the pure amorphous and pure crystalline phases of regioregular p3ht, *Macromolecules*, 2013, **46**(6), 2450–2467.
51. Falk May, Mustapha Al-Helwi, Björn Baumeier, Wolfgang Kowalsky, Evelyn Fuchs, Christian Lennartz and Denis Andrienko, Design rules for charge-transport efficient host materials for phosphorescent organic light-emitting diodes, *J. Am. Chem. Soc.*, 2012, **134**(33), 13818–13822.

52. Falk May, Björn Baumeier, Christian Lennartz and Denis Andrienko, Can lattice models predict the density of states of amorphous organic semiconductors?, *Phys. Rev. Lett.*, 2012, **109**(13), 136401.
53. Patrick Gemünden, Carl Poelking, Kurt Kremer, Denis Andrienko and Kostas Ch, Daoulas. Nematic ordering, conjugation, and density of states of soluble polymeric semiconductors, *Macromolecules*, 2013, **46**(14), 5762–5774.
54. W. G. Noid, J. Chu, G. S. Ayton, V. Krishna, S. Izvekov, G. A. Voth, A. Das and H. C. Andersen, The multiscale coarse graining method. 1. a rigorous bridge between atomistic and coarse-grained models, *J. Chem. Phys.*, 2008, **128**, 244114.
55. Victor Rühle, Christoph Junghans, Alexander Lukyanov, Kurt Kremer and Denis Andrienko, Versatile object-oriented toolkit for coarse-graining applications, *J. Chem. Theory. Comput.*, 2009, **5**(12), 3211–3223.
56. A. K. Soper, Empirical potential Monte Carlo simulation of fluid structure, *Chem. Phys.*, 1996, **202**, 295–306.
57. Alexander P. Lyubartsev and Aatto Laaksonen, Calculation of effective interaction potentials from radial distribution functions: A reverse Monte Carlo approach, *Phys. Rev. E*, 1995, **52**(4), 3730–3737.
58. D. Reith, M. Pütz and F. Müller-Plathe, Deriving effective mesoscale potentials from atomistic simulations, *J. Comp. Chem.*, 2003, **24**(13), 1624–1636.
59. Mara Jochum, Denis Andrienko, Kurt Kremer and Christine Peter, Structure-based coarse-graining in liquid slabs, *J. Chem. Phys.*, 2012, **137**(6), 064102.
60. F. Ercolessi and J. B. Adams, Interatomic potentials from 1st-principles calculations - the force-matching method, *Europhys. Lett.*, 1994, **26**(8), 583–588.
61. S. Izvekov, M. Parrinello, C. J. Burnham and G. A. Voth, Effective force fields for condensed phase systems from ab initio molecular dynamics simulation: A new method for force-matching, *J. Chem. Phys.*, 2004, **120**(23), 10896–10913.
62. M. Scott Shell, The relative entropy is fundamental to multiscale and inverse thermodynamic problems, *J. Chem. Phys.*, 2008, **129**(14), 144108.
63. W. G. Noid, J. W. Chu, G. S. Ayton and G. A. Voth, Multiscale coarse-graining and structural correlations: Connections to liquid-state theory, *J. Phys. Chem. B*, 2007, **111**(16), 4116–4127.
64. W. G. Noid, Perspective: Coarse-grained models for biomolecular systems, *J. Chem. Phys.*, 2013, **139**(9), 090901.
65. Khanh Do, David M. Huang, Roland Faller and Adam J. Moulé, A comparative MD study of the local structure of polymer semiconductors p3ht and PBTTT, *Phys. Chem. Chem. Phys.*, 2010, **12**(44), 14735.

66. David M. Huang, Roland Faller, Khanh Do and Adam J. Moulé, Coarse-grained computer simulations of polymer/fullerene bulk heterojunctions for organic photovoltaic applications, *J. Chem. Theory. Comput.*, 2010, **6**(2), 526–537.
67. Cheng-Kuang Lee, Chun-Wei Pao and Chih-Wei Chu, Multiscale molecular simulations of the nanoscale morphologies of p3ht:PCBM blends for bulk heterojunction organic photovoltaic cells, *Energy & Environmental Science*, 2011, **4**(10), 4124–4132.
68. Eric Jankowski, Hilary S. Marsh and Arthi Jayaraman, Computationally linking molecular features of conjugated polymers and fullerene derivatives to bulk heterojunction morphology, *Macromolecules*, 2013, **46**(14), 5775–5785.
69. V. Rühle, J. Kirkpatrick, K. Kremer and D. Andrienko, Coarse-grained modelling of polypyrrole morphologies, *Phys. Stat. Solidi B*, 2008, **245**, 844.
70. Kyra N. Schwarz, Tak W. Kee and David M. Huang, Coarse-grained simulations of the solution-phase self-assembly of poly(3-hexylthiophene) nanostructures, *Nanoscale*, 2013, **5**(5), 2017–2027.
71. Kostas Ch Daoulas and Marcus Müller, Comparison of simulations of lipid membranes with membranes of block copolymers. In Wolfgang Peter Meier and Wolfgang Knoll, editors, *Polymer Membranes/Biomembranes, number 224 in Advances in Polymer Science*, pages 43–85. Springer, Berlin, Heidelberg, 2010.
72. Marcus Müller, Studying amphiphilic self-assembly with soft coarse-grained models, *J. Stat. Phys.*, 2011, **145**(4), 967–1016.
73. Gavin A. Buxton and Nigel Clarke, Predicting structure and property relations in polymeric photovoltaic devices, *Phys. Rev. B*, 2006, **74**(8), 085207.
74. Anton Pershin, Sergii Donets and Stephan A. Baeurle, A new multiscale modeling method for simulating the loss processes in polymer solar cell nanodevices, *J. Chem. Phys.*, 2012, **136**(19), 194102.
75. Sergii Donets, Anton Pershin, Martin J. A. Christlmaier and Stephan A. Baeurle, A multiscale modeling study of loss processes in block-copolymer-based solar cell nanodevices, *J. Chem. Phys.*, 2013, **138**(9), 094901.
76. Manas Shah and Venkat Ganesan, Correlations between morphologies and photovoltaic properties of rod-coil block copolymers, *Macromolecules*, 2010, **43**(1), 543–552.
77. Hari K. Kodali and Baskar Ganapathysubramanian, A computational framework to investigate charge transport in heterogeneous organic photovoltaic devices, *Comput. Methods Appl. Mech. Eng.*, 2012, **247–248**, 113–129.
78. J. A. Barker, C. M. Ramsdale and N. C. Greenham, Modeling the current–voltage characteristics of bilayer polymer photovoltaic devices, *Phys. Rev. B*, 2003, **67**(7), 075205.

79. C. M. Martin, V. M. Burlakov, H. E. Assender and D. A. R. Barkhouse, A numerical model for explaining the role of the interface morphology in composite solar cells, *J. Appl. Phys.*, 2007, **102**(10), 104506.
80. Robin G. E. Kimber, Edward N. Wright, Simon E. J. O'Kane, Alison B. Walker and James C. Blakesley, Mesoscopic kinetic Monte Carlo modeling of organic photovoltaic device characteristics, *Phys. Rev. B*, 2012, **86**(23), 235206.
81. Y. C. Cheng, R. J. Silbey, D. A. da Silva Filho, J. P. Calbert, J. Cornil and J. L. Brédas, Three-dimensional band structure and bandlike mobility in oligoacene single crystals: A theoretical investigation, *J. Chem. Phys.*, 2003, **118**(8), 3764–3774.
82. Yanting Yang, Yanming Yang, Fugen Wu and Zhigang Wei, First-principles electronic structure of copper phthalocyanine (CuPc), *Solid State Communications*, 2008, **148**(11–12), 559–562.
83. Edgar A. Silinsh and Vladislav Capek. *Organic Molecular Crystals: Interacton Localization, and Transport Phenomena*. American Institute of Physics, 1 edition, 1997.
84. Yuan-Chung Cheng and Robert J. Silbey, A unified theory for charge-carrier transport in organic crystals, *J. Chem. Phys.*, 2008, **128**(11), 114713.
85. J. L. Brédas, J. P. Calbert, D. A. da Silva Filho and J. Cornil, Organic semiconductors: A theoretical characterization of the basic parameters governing charge transport, *Proc. Natl. Acad. Sci. USA*, 2002, **99**(9), 5804–5809.
86. Veaceslav Coropceanu, Jérôme Cornil, Demetrio A. da Silva Filho, Yoann Olivier, Robert Silbey and Jean-Luc Brédas, Charge transport in organic semiconductors, *Chem. Rev.*, 2007, **107**(4), 926–952.
87. James Kirkpatrick, An approximate method for calculating transfer integrals based on the ZINDO hamiltonian, *Int. J. Quantum Chem.*, 2008, **108**(1), 51–56.
88. Björn Baumeier, James Kirkpatrick and Denis Andrienko, Density-functional based determination of intermolecular charge transfer properties for large-scale morphologies, *Phys. Chem. Chem. Phys.*, 2010, **12**(36), 11103.
89. Troy Van Voorhis, Tim Kowalczyk, Benjamin Kaduk, Lee-Ping Wang, Chiao-Lun Cheng and Qin Wu, The diabatic picture of electron transfer, reaction barriers, and molecular dynamics, *Annual Review of Physical Chemistry*, 2010, **61**(1), 149–170.
90. S. F. Boys, Construction of some molecular orbitals to be approximately invariant for changes from one molecule to another, *Rev. Mod. Phys.*, 1960, **32**(2), 296–299.
91. Michael Baer, Adiabatic and diabatic representations for atom-molecule collisions: Treatment of the collinear arrangement, *Chem. Phys. Lett.*, 1975, **35**(1), 112–118.

92. Robert J. Cave and Marshall D. Newton, Generalization of the Mulliken-Hush treatment for the calculation of electron transfer matrix elements, *Chem. Phys. Lett.*, 1996, **249**(1–2), 15–19.
93. Gregory J. Atchity and Klaus Ruedenberg, Determination of diabatic states through enforcement of configurational uniformity, *Theoretical Chemistry Accounts*, 1997, **97**(1–4), 47–58.
94. C. Alden Mead and Donald G. Truhlar, Conditions for the definition of a strictly diabatic electronic basis for molecular systems, *J. Chem. Phys.*, 1982, 77(12), 6090–6098.
95. T. Pacher, L. S. Cederbaum and H. Köppel, Approximately diabatic states from block diagonalization of the electronic hamiltonian, *J. Chem. Phys.*, 1988, **89**(12), 7367–7381.
96. Eugene S. Kryachko, On generalized Mulliken–Hush approach of electronic transfer: Inclusion of non-zero off-diagonal diabatic dipole moment, *J. Phys. Chem. A*, 1999, **103**(22), 4368–4370.
97. Hisao Nakamura and Donald G. Truhlar, The direct calculation of diabatic states based on configurational uniformity, *J. Chem. Phys.*, 2001, **115**(22), 10353–10372.
98. Joseph E. Subotnik, Sina Yeganeh, Robert J. Cave and Mark A. Ratner, Constructing diabatic states from adiabatic states: Extending generalized Mulliken–Hush to multiple charge centers with Boys localization, *J. Chem. Phys.*, 2008, **129**(24), 244101.
99. Chao-Ping Hsu, The electronic couplings in electron transfer and excitation energy transfer, *Accounts Chem. Res.*, 2009, **42**(4), 509–518.
100. Xiaolei Zhu and David R. Yarkony, Toward eliminating the electronic structure bottleneck in nonadiabatic dynamics on the fly: An algorithm to fit nonlocal, quasidiabatic, coupled electronic state hamiltonians based on ab initio electronic structure data, *J. Chem. Phys.*, 2010, **132**(10), 104101.
101. Michele Pavanello and Johannes Neugebauer, Linking the historical and chemical definitions of diabatic states for charge and excitation energy transfer reactions in condensed phase, *J. Chem. Phys.*, 2011, **135**(13), 134113.
102. Elisabetta Collini and Gregory D. Scholes, Coherent intrachain energy migration in a conjugated polymer at room temperature, *Science*, 2009, **323**(5912), 369–373.
103. Alberto Salleo, R. Joseph Kline, Dean M. DeLongchamp and Michael L. Chabinyc, Microstructural characterization and charge transport in thin films of conjugated polymers, *Adv. Mater.*, 2010, **22**(34), 3812–3838.
104. D. Beljonne, J. Cornil, H. Sirringhaus, P. J. Brown, M. Shkunov, R. H. Friend and J.-L. Brédas, Optical signature of delocalized polarons in conjugated polymers, *Adv. Funct. Mater.*, 2001, **11**(3), 229–234.
105. Peter J. Brown, Henning Sirringhaus, Mark Harrison, Maxim Shkunov and Richard H. Friend, Optical spectroscopy of field-induced charge in

self-organized high mobility poly(3-hexylthiophene), *Phys. Rev. B*, 2001, **63**(12), 125204.
106. Nenad Vukmirović and Lin-Wang Wang, Density of states and wave function localization in disordered conjugated polymers: A large scale computational study, *J. Phys. Chem. B*, 2011, **115**(8), 1792–1797.
107. Sanjio S. Zade, Natalia Zamoshchik and Michael Bendikov, From short conjugated oligomers to conjugated polymers. lessons from studies on long conjugated oligomers, *Accounts Chem. Res.*, 2011, **44**(1), 14–24.
108. Iffat H. Nayyar, Enrique R. Batista, Sergei Tretiak, Avadh Saxena, Darryl L. Smith and Richard L. Martin, Role of geometric distortion and polarization in localizing electronic excitations in conjugated polymers, *J. Chem. Theory. Comput.*, 2013, **9**(2), 1144–1154.
109. Hugo Bronstein, Zhuoying Chen, Raja Shahid Ashraf, Weimin Zhang, Junping Du, James R. Durrant, Pabitra Shakya Tuladhar, Kigook Song, Scott E. Watkins, Yves Geerts, Martijn M. Wienk, Rene A. J. Janssen, Thomas Anthopoulos, Henning Sirringhaus, Martin Heeney and Iain McCulloch, Thieno[3,2-b]thiophene-diketopyrrolopyrrole-containing polymers for high-performance organic field-effect transistors and organic photovoltaic devices, *J. Am. Chem. Soc.*, 2011, **133**(10), 3272–3275.
110. Edward H. Magin and Paul M. Borsenberger, Electron transport in n,n'-bis(2-phenethyl)-perylene-3,4: 9,10-bis(dicarboximide), *J. Appl. Phys.*, 1993, **73**(2), 787–791.
111. Mark Van der Auweraer, Frans C. De Schryver, Paul M. Borsenberger and Heinz Bässler, Disorder in charge transport in doped polymers, *Adv. Mater.*, 1994, **6**(3), 199–213.
112. Jui-Fen Chang, Jenny Clark, Ni Zhao, Henning Sirringhaus, Dag W. Breiby, Jens W. Andreasen, Martin M. Nielsen, Mark Giles, Martin Heeney and Iain McCulloch, Molecular-weight dependence of interchain polaron delocalization and exciton bandwidth in high-mobility conjugated polymers, *Phys. Rev. B*, 2006, **74**(11), 115318.
113. Ting Qin and Alessandro Troisi, Relation between structure and electronic properties of amorphous MEH-PPV polymers, *J. Am. Chem. Soc.*, 2013, **135**(30), 11247–11256.
114. S. Shaked, S. Tal, Y. Roichman, A. Razin, S. Xiao, Y. Eichen and N. Tessler, Charge density and film morphology dependence of charge mobility in polymer field-effect transistors, *Adv. Mater.*, 2003, **15**(11), 913–916.
115. Mark S. Gordon, Jonathan M. Mullin, Spencer R. Pruitt, Luke B. Roskop, Lyudmila V. Slipchenko and Jerry A. Boatz, Accurate methods for large molecular systems, *J. Phys. Chem. B*, 2009, **113**(29), 9646–9663.
116. Chris-Kriton Skylaris, Peter D. Haynes, Arash A. Mostofi and Mike C. Payne, Introducing ONETEP: Linear-scaling density functional simulations on parallel computers, *J. Chem. Phys.*, 2005, **122**(8), 084119.

117. José M. Soler, Emilio Artacho, Julian D. Gale, Alberto García, Javier Junquera, Pablo Ordejón and Daniel Sánchez-Portal, The SIESTA method for ab initio order-n materials simulation, *J. Phys-Condens. Mat.*, 2002, **14**(11), 2745.
118. David P. McMahon and Alessandro Troisi, An ad hoc tight binding method to study the electronic structure of semiconducting polymers, *Chem. Phys. Lett.*, 2009, **480**(4–6), 210–214.
119. Nenad Vukmirović and Lin-Wang Wang, Electronic structure of disordered conjugated polymers: Polythiophenes, *J. Phys. Chem. B*, 2009, **113**(2), 409–415.
120. Nenad Vukmirović and Lin-Wang Wang, Charge carrier motion in disordered conjugated polymers: A multiscale ab initio study, *Nano Letters*, 2009, **9**(12), 3996–4000.
121. Dmitri G. Fedorov and Kazuo Kitaura, Extending the power of quantum chemistry to large systems with the fragment molecular orbital method, *J. Phys. Chem. A*, 2007, **111**(30), 6904–6914.
122. Kazuo Kitaura, Eiji Ikeo, Toshio Asada, Tatsuya Nakano and Masami Uebayasi, Fragment molecular orbital method: an approximate computational method for large molecules, *Chem. Phys. Lett.*, 1999, **313**(3–4), 701–706.
123. Tomáš Kubař and Marcus Elstner, A hybrid approach to simulation of electron transfer in complex molecular systems, *Journal of The Royal Society Interface*, 2013, **10**(87), 20130415.
124. Jiangang Liu, Yue Sun, Xiang Gao, Rubo Xing, Lidong Zheng, Shupeng Wu, Yanhou Geng and Yanchun Han, Oriented poly(3-hexylthiophene) nanofibril with the π–π stacking growth direction by solvent directional evaporation, *Langmuir*, 2011, **27**(7), 4212–4219.
125. D. Porezag, Th. Frauenheim, Th. Köhler, G. Seifert and R. Kaschner, Construction of tight-binding-like potentials on the basis of density-functional theory: Application to carbon, *Phys. Rev. B*, 1995, **51**(19), 12947–12957.
126. M. Elstner, D. Porezag, G. Jungnickel, J. Elsner, M. Haugk, Th. Frauenheim, S. Suhai and G. Seifert, Self-consistent-charge density-functional tight-binding method for simulations of complex materials properties, *Phys. Rev. B*, 1998, **58**(11), 7260–7268.
127. Tao Liu and Alessandro Troisi, Understanding the microscopic origin of the very high charge mobility in PBTTT: Tolerance of thermal disorder, *Adv. Funct. Mater.*, 2014, **24**(7), 925–933.
128. Åsa Johansson and Sven Stafström, Polaron dynamics in a system of coupled conjugated polymer chains, *Phys. Rev. Lett.*, 2001, **86**(16), 3602–3605.
129. William Barford and David Trembath, Exciton localization in polymers with static disorder, *Phys. Rev. B*, 2009, **80**(16), 165418.
130. Nenad Vukmirović and Lin-Wang Wang, Carrier hopping in disordered semiconducting polymers: How accurate is the Miller–Abrahams model?, *Appl. Phys. Lett.*, 2010, **97**(4), 043305.

131. Allen Miller and Elihu Abrahams, Impurity conduction at low concentrations, *Phys. Rev.*, 1960, **120**(3), 745–755.
132. Nenad Vukmirović, A comparative study of electronic properties of disordered conjugated polymers, *Phys. Chem. Chem. Phys.*, 2013, **15**(10), 3543–3551.
133. Franz X. Bronold, Andreas Alvermann and Holger Fehske, Anderson localization in strongly coupled disordered electron–phonon systems, *Philosophical Magazine*, 2004, **84**(7), 673–704.
134. R. Fornari and Alessandro Troisi, Theory of charge hopping along a disordered polymer chain, *Phys. Chem. Chem. Phys.*, 2014, **16**, 9997–10007.
135. Carl Poelking, Kostas Daoulas, Alessandro Troisi and Denis Andrienko, Morphology and charge transport in p3ht: A theorist's perspective, *Adv. Polym. Sci.*, 2014.
136. Rudolph Marcus, Electron transfer reactions in chemistry. Theory and experiment, *Rev. Mod. Phys.*, 1993, **65**(3), 599–610.
137. Volkhard May and Oliver Kühn. *Charge and Energy Transfer Dynamics in Molecular Systems*. Wiley-VCH, 3rd, revised and enlarged edition, 2011.
138. Hermann Grabert and Ulrich Weiss, Quantum tunneling rates for asymmetric double-well systems with ohmic dissipation, *Phys. Rev. Lett.*, 1985, **54**(15), 1605–1608.
139. Matthew P. A. Fisher and Alan T. Dorsey, Dissipative quantum tunneling in a biased double-well system at finite temperatures, *Phys. Rev. Lett.*, 1985, **54**(15), 1609–1612.
140. Victor Rühle, Alexander Lukyanov, Falk May, Manuel Schrader, Thorsten Vehoff, James Kirkpatrick, Björn Baumeier and Denis Andrienko, Microscopic simulations of charge transport in disordered organic semiconductors, *J. Chem. Theory. Comput.*, 2011, **7**(10), 3335–3345.
141. Kamal Asadi, Auke J. Kronemeijer, Tobias Cramer, L. Jan Anton Koster, Paul W. M. Blom and Dago M. de Leeuw, Polaron hopping mediated by nuclear tunnelling in semiconducting polymers at high carrier density, *Nature Communications*, 2013, **4**, 1710.
142. E. F. Valeev, V. Coropceanu, D. A. da Silva Filho, S. Salman and J.-L. Bredas, Effect of electronic polarization on charge-transport parameters in molecular organic semiconductors, *J. Am. Chem. Soc.*, 2006, **128**(30), 9882.
143. Xinliang Feng, Valentina Marcon, Wojciech Pisula, Michael Ryan Hansen, James Kirkpatrick, Ferdinand Grozema, Denis Andrienko, Kurt Kremer and Klaus Müllen, Towards high charge-carrier mobilities by rational design of the shape and periphery of discotics, *Nat. Mater.*, 2009, **8**(5), 421–426.
144. Carl Poelking, Eunkyung Cho, Alexander Malafeev, Viktor Ivanov, Kurt Kremer, Chad Risko, Jean-Luc Brédas and Denis Andrienko, Characterization of charge-carrier transport in semicrystalline polymers: Electronic couplings, site energies, and charge-carrier dynamics

in poly(bithiophene-alt-thienothiophene) PBTTT, *J. Phys. Chem. C*, 2013, **117**(4), 1633–1640.
145. Y. Olivier, L. Muccioli, V. Lemaur, Y. H. Geerts, C. Zannoni and J. Cornil, Theoretical characterization of the structural and hole transport dynamics in liquid-crystalline phthalocyanine stacks, *J. Phys. Chem. B*, 2009, **113**(43), 14102.
146. J. R. Reimers, A practical method for the use of curvilinear coordinates in calculations of normal-mode-projected displacements and Duschinsky rotation matrices for large molecules, *J. Chem. Phys.*, 9103, **115**(20), 2001.
147. Manuel Schrader, Roland Fitzner, Moritz Hein, Chris Elschner, Björn Baumeier, Karl Leo, Moritz Riede, Peter Bäuerle and Denis Andrienko, Comparative study of microscopic charge dynamics in crystalline acceptor-substituted oligothiophenes, *J. Am. Chem. Soc.*, 2012, **134**(13), 6052–6056.
148. Christof Hättig, Recurrence relations for the direct calculation of spherical multipole interaction tensors and coulomb-type interaction energies, *Chem. Phys. Lett.*, 1996, **260**(3–4), 341–351.
149. Christof Hättig and Bernd Artur Heß, Calculation of orientation-dependent double-tensor moments for coulomb-type intermolecular interactions, *Molecular Physics*, 1994, **81**(4), 813–824.
150. Toon Verstraelen, Ewald Pauwels, Frank De Proft, Veronique Van Speybroeck, Paul Geerlings and Michel Waroquier, Assessment of atomic charge models for gas-phase computations on polypeptides, *J. Chem. Theory. Comput.*, 2012, **8**(2), 661–676.
151. Curt M. Breneman and Kenneth B. Wiberg, Determining atom-centered monopoles from molecular electrostatic potentials. the need for high sampling density in formamide conformational analysis, *J. Comput. Chem.*, 1990, **11**(3), 361–373.
152. A. J. Stone and M. Alderton, Distributed multipole analysis, *Molecular Physics*, 1985, **56**(5), 1047–1064.
153. Anthony J. Stone, Distributed multipole analysis: stability for large basis sets, *J. Chem. Theory Comput.*, 2005, **1**(6), 1128–1132.
154. Lisa Emily Chirlian and Michelle Miller Francl, Atomic charges derived from electrostatic potentials: a detailed study, *J. Comput. Chem.*, 1987, **8**(6), 894–905.
155. B. T. Thole, Molecular polarizabilities calculated with a modified dipole interaction, *Chem. Phys.*, 1981, **59**(3), 341–350.
156. Piet Th. van Duijnen and Marcel Swart, Molecular and atomic polarizabilities: Thole's model revisited, *J. Phys. Chem. A*, 1998, **102**(14), 2399–2407.
157. Jon Applequist, James R. Carl and Kwok-Kueng Fung, Atom dipole interaction model for molecular polarizability. Application to polyatomic molecules and determination of atom polarizabilities, *J. Am. Chem. Soc.*, 1972, **94**(9), 2952–2960.

158. Pengyu Ren and Jay W. Ponder, Polarizable atomic multipole water model for molecular mechanics simulation, *J. Phys. Chem. B*, 2003, **107**(24), 5933–5947.
159. Manuel Schrader, Christian Körner, Chris Elschner and Denis Andrienko, Charge transport in amorphous and smectic mesophases of dicyanovinyl-substituted oligothiophenes, *J. Mater. Chem.*, 2012, **22**(41), 22258–22264.
160. Sergey V. Novikov and Anatoly V. Vannikov, Cluster structure in the distribution of the electrostatic potential in a lattice of randomly oriented dipoles, *J. Phys. Chem.*, 1995, **99**(40), 14573–14576.
161. S. Novikov, D. Dunlap, V. Kenkre, P. Parris and A. Vannikov, Essential role of correlations in governing charge transport in disordered organic materials, *Phys. Rev. Lett.*, 1998, **81**(20), 4472–4475.
162. D. Dunlap, P. Parris and V. Kenkre, Charge–dipole model for the universal field dependence of mobilities in molecularly doped polymers, *Phys. Rev. Lett.*, 1996, **77**(3), 542–545.
163. Mathieu Linares, David Beljonne, Jerome Cornil, Kelly Lancaster, J.-L. Brédas, Stijn Verlaak, Alexander Mityashin, Paul Heremans, Andreas Fuchs, Christian Lennartz, Julien Idé, Raphael Méreau, Philippe Aurel, Laurent Ducasse and Frederic Castet, On the interface dipole at the pentacene-fullerene heterojunction: a theoretical study, *J. Phys. Chem. C*, 2010, **114**(7), 3215–3224.
164. Stijn Verlaak, David Beljonne, David Cheyns, Cedric Rolin, Mathieu Linares, Frédéric Castet, Jérôme Cornil and Paul Heremans, Electronic structure and geminate pair energetics at organic-organic interfaces: The case of pentacene/c60 heterojunctions, *Adv. Funct. Mater.*, 2009, **19**(23), 3809–3814.
165. Stijn Verlaak and Paul Heremans, Molecular microelectrostatic view on electronic states near pentacene grain boundaries, *Phys. Rev. B*, 2007, **75**(11), 115127.
166. Shane R. Yost, Lee-Ping Wang and Troy Van Voorhis, Molecular insight into the energy levels at the organic donor/acceptor interface: a quantum mechanics/molecular mechanics study, *J. Phys. Chem. C*, 2011, **115**(29), 14431–14436.
167. Shane R. Yost and Troy Van Voorhis, Electrostatic effects at organic semiconductor interfaces: A mechanism for ''cold'' exciton breakup, *J. Phys. Chem. C*, 2013, **117**(11), 5617–5625.
168. Sébastien Mothy, Maxime Guillaume, Julien Idé, Frédéric Castet, Laurent Ducasse, Jérôme Cornil and David Beljonne, Tuning the interfacial electronic structure at organic heterojunctions by chemical design, *J. Phys. Chem. Lett.*, 2012, **3**(17), 2374–2378.
169. Julien Idé, Sébastien Mothy, Adrien Savoyant, Alain Fritsch, Philippe Aurel, Raphaël Méreau, Laurent Ducasse, Jérôme Cornil, David Beljonne and Frédéric Castet, Interfacial dipole and band

bending in model pentacene/c60 heterojunctions, *Int. J. Quantum Chem.*, 2013, **113**(4), 580–584.
170. Ralf Mauer, Marcel Kastler and Frédéric Laquai, The impact of polymer regioregularity on charge transport and efficiency of p3ht:PCBM photovoltaic devices, *Adv. Funct. Mater.*, 2010, **20**(13), 2085–2092.
171. Amy M. Ballantyne, Lichun Chen, Justin Dane, Thomas Hammant, Felix M. Braun, Martin Heeney, Warren Duffy, Iain McCulloch, Donal D. C. Bradley and Jenny Nelson, The effect of poly(3-hexylthiophene) molecular weight on charge transport and the performance of polymer:fullerene solar cells, *Adv. Funct. Mater.*, 2008, **18**(16), 2373–2380.
172. J. Cottaar and P. A. Bobbert, Calculating charge-carrier mobilities in disordered semiconducting polymers: Mean field and beyond, *Phys. Rev. B*, 2006, **74**(11), 115204.
173. J. Kirkpatrick, V. Marcon, J. Nelson, K. Kremer and D. Andrienko, Charge mobility of discotic mesophases: a multiscale quantum and classical study, *Phys. Rev. Lett.*, 2007, **98**(22), 227402.
174. Falk May, Valentina Marcon, Michael Ryan Hansen, Ferdinand Grozema and Denis Andrienko, Relationship between supramolecular assembly and charge-carrier mobility in perylenediimide derivatives: the impact of side chains, *J. Mater. Chem.*, 2011, **21**(26), 9538.
175. Yi-Kang Lan, Cheng Han Yang and Hsiao-Ching Yang, Theoretical investigations of electronic structure and charge transport properties in polythiophene-based organic field-effect transistors, *Polymer International*, 2010, **59**(1), 16–21.
176. H. Scher, S. Alexander and E. W. Montroll, Field-induced trapping as a probe of dimensionality in molecular crystals, *Proc. Natl. Acad. Sci. USA*, 1980, **77**(7), 3758–3762.
177. V. Marcon, J. Kirkpatrick, W. Pisula and D. Andrienko, Supramolecular structure of perylene tetracarboxdiimides, *Phys. Status Solidi B*, 2008, **245**(5), 820–824.
178. Denis Andrienko, James Kirkpatrick, Valentina Marcon, Jenny Nelson and Kurt Kremer, Structure–charge mobility relation for hexabenzocoronene derivatives, *Phys. Status Solidi B*, 2008, **245**(5), 830–834.
179. Jenny Nelson, Joe J. Kwiatkowski, James Kirkpatrick and Jarvist M. Frost, Modeling charge transport in organic photovoltaic materials, *Accounts Chem. Res.*, 2009, **42**(11), 1768–1778.
180. P. M. Borsenberger, L. Pautmeier and H. Bässler, Charge transport in disordered molecular solids, *J. Chem. Phys.*, 1991, **94**(8), 5447.
181. P. Borsenberger, L. Pautmeier and H. Bässler, Nondispersive-to-dispersive charge-transport transition in disordered molecular solids, *Phys. Rev. B*, 1992, **46**(19), 12145–12153.
182. P. M. Borsenberger, E. H. Magin, M. Der VanAuweraer and F. C. De Schryver, The role of disorder on charge transport in molecularly doped

polymers and related materials, *Physica Status Solidi (a)*, 1993, **140**(1), 9–47.
183. Alexander Lukyanov and Denis Andrienko, Extracting nondispersive charge carrier mobilities of organic semiconductors from simulations of small systems, *Phys. Rev. B*, 2010, **82**(19), 193202.
184. Bernard Derrida, Velocity and diffusion constant of a periodic one-dimensional hopping model, *J. Stat. Phys.*, 1983, **31**(3), 433–450.
185. Kazuhiko Seki and M. Tachiya, Electric field dependence of charge mobility in energetically disordered materials: Polaron aspects, *Phys. Rev. B*, 2001, **65**(1), 014305.
186. Pascal Kordt, Ole Stenzel, Björn Baumeier, Volker Schmidt and Denis Andrienko, Parametrization of extended gaussian disorder models from microscopic charge transport simulations, *J. Chem. Theory. Comput.*, 2014, **10**(6), 2508–2513.
187. J. Cottaar, L. J. A. Koster, R. Coehoorn and P. A. Bobbert, Scaling theory for percolative charge transport in disordered molecular semiconductors, *Phys. Rev. Lett.*, 2011, **107**(13), 136601.
188. Y. Yimer, P. Bobbert and R. Coehoorn, Charge transport in disordered organic host's guest systems: Effects of carrier density and electric field, *Synthetic Metals*, 2399, **159**(21–22), 2009.
189. J. A. Freire and C. Tonezer, Density of states and energetic correlation in disordered molecular systems due to induced dipoles, *J. Chem. Phys.*, 2009, **130**(13), 134901.
190. J. J. M. van der Holst, F. W. A. van Oost, R. Coehoorn and P. A. Bobbert, Monte Carlo study of charge transport in organic sandwich-type single-carrier devices: Effects of Coulomb interactions, *Phys. Rev. B*, 2011, **83**(8), 085206.
191. B. Baumeier, O. Stenzel, C. Poelking, D. Andrienko and V. Schmidt, Stochastic modeling of molecular charge transport networks, *Phys. Rev. B*, 2012, **86**(18), 184202.
192. T. Brereton, O. Stenzel, B. Baumeier, D. Andrienko, V. Schmidt and D. Kroese, Efficient Simulation of Markov chains using segmentation, *Methodology Comput. Appl. Probability*, 2014, **16**(2), 465.
193. O. Stenzel, C. Hirsch, T. Brereton, B. Baumeier, D. Andrienko, D. P. Kroese, V. Schmidt, A generalized toolkit for studying the charge transport properties of materials via random walks in random environments, submitted.
194. P. P. Ewald, Die berechnung optischer und elektrostatischer gitterpotentiale, *Annalen der Physik*, 1921, **369**(3), 253–287.
195. Carl Poelking, Max Tietze, Chris Elschner, Karl Leo, Björn Baumeier, Denis Andrienko, Decisive role of long-range interactions and mesoscopic order at organic interfaces, submitted, 2014.
196. E. R. Smith, Electrostatic energy in ionic crystals, *Proceedings of the Royal Society of London. A. Mathematical and Physical Sciences*, 1981, **375**(1763), 475–505.

197. A. Wilke, P. Amsalem, J. Frisch, B. Bröker, A. Vollmer and N. Koch, Electric fields induced by energy level pinning at organic heterojunctions, *Appl. Phys. Lett.*, 2011, **98**(12), 123304.
198. David Beljonne, Jérôme Cornil, Luca Muccioli, Claudio Zannoni, Jean-Luc Brédas and Frédéric Castet, Electronic processes at organic-organic interfaces: insight from modeling and implications for opto-electronic devices, *Chem. Mater.*, 2011, **23**(3), 591–609.
199. David P. McMahon, David L. Cheung and Alessandro Troisi, Why holes and electrons separate so well in polymer/fullerene photovoltaic cells, *J. Phys. Chem. Lett.*, 2011, **2**(21), 2737–2741.
200. A. Liu, S. Zhao, S.-B. Rim, J. Wu, M. Könemann, P. Erk and P. Peumans, Control of electric field strength and orientation at the donor–acceptor interface in organic solar cells, *Adv. Mater.*, 2008, **20**(5), 1065–1070.
201. Brian A. Gregg, Entropy of charge separation in organic photovoltaic cells: The benefit of higher dimensionality, *J. Phys. Chem. Lett.*, 2011, **2**(24), 3013–3015.
202. Askat E. Jailaubekov, Adam P. Willard, John R. Tritsch, Wai-Lun Chan, Na Sai, Raluca Gearba, Loren G. Kaake, Kenrick J. Williams, Kevin Leung, Peter J. Rossky and X.-Y. Zhu, Hot charge-transfer excitons set the time limit for charge separation at donor/acceptor interfaces in organic photovoltaics, *Nat. Mater.*, 2013, **12**(1), 66–73.
203. Domenico Caruso and Alessandro Troisi, Long-range exciton dissociation in organic solar cells, *Proc. Natl. Acad. Sci. USA*, 2012, **109**(34), 13498–13502.
204. Erich Runge and E. K. U. Gross, Density-functional theory for time-dependent systems, *Phys. Rev. Lett.*, 1984, **52**(12), 997–1000.
205. Zheng-Li Cai, Karina Sendt and Jeffrey R. Reimers, Failure of density-functional theory and time-dependent density-functional theory for large extended π systems, *J. Chem. Phys.*, 2002, **117**, 5543.
206. Eneritz Muguruza González, Leonardo Guidoni and Carla Molteni, Chemical and protein shifts in the spectrum of the photoactive yellow protein: a time-dependent density functional theory/molecular mechanics study, *Phys. Chem. Chem. Phys.*, 2009, **11**, 4556.
207. David J Tozer, Relationship between long-range charge-transfer excitation energy error and integer discontinuity in Kohn–Sham theory, *J. Chem. Phys.*, 2003, **119**(24), 12697–12699.
208. Andreas Dreuw and Martin Head-Gordon, Failure of time-dependent density functional theory for long-range charge-transfer excited states: The zincbacteriochlorin-bacteriochlorin and bacteriochlorophyll-spheroidene complexes, *J. Am. Chem. Soc.*, 2004, **126**(12), 4007–4016.
209. Roberto Peverati and Donald G. Truhlar, Improving the accuracy of hybrid meta-GGA density functionals by range separation, *J. Phys. Chem. Lett.*, 2011, **2**(21), 2810–2817.
210. A. Karolewski, T. Stein, R. Baer and S. Kümmel, Communication: Tailoring the optical gap in light-harvesting molecules, *J. Chem. Phys.*, 2011, **134**(15), 151101–151101–4.

211. Tamar Stein, Leeor Kronik and Roi Baer, Reliable prediction of charge transfer excitations in molecular complexes using time-dependent density functional theory, *J. Am. Chem. Soc.*, 2009, **131**(8), 2818–2820.
212. John S. Sears, Thomas Koerzdoerfer, Cai-Rong Zhang and Jean-Luc Brédas, Communication: Orbital instabilities and triplet states from time-dependent density functional theory and long-range corrected functionals, *J. Chem. Phys.*, 2011, **135**(15), 151103–151103–4.
213. Mathias Pabst, Dage Sundholm and Andreas Köhn, Ab initio studies of triplet-state properties for organic semiconductor molecules, *J. Phys. Chem. C*, 2012, **116**(29), 15203–15217.
214. Itamar Borges, Adélia J. A. Aquino, Andreas Köhn, Reed Nieman, William L. Hase, Lin X. Chen and Hans Lischka, Ab initio modeling of excitonic and charge-transfer states in organic semiconductors: The PTB1/PCBM low band gap system, *J. Am. Chem. Soc.*, 2013, **135**(49), 18252–18255.
215. Bernd Lunkenheimer and Andreas Köhn, Solvent effects on electronically excited states using the conductor-like screening model and the second-order correlated method ADC(2), *J. Chem. Theory. Comput.*, 2013, **9**(2), 977–994.
216. L. Hedin and S. Lundqvist, Effects of electron-electron and electron–phonon interactions on the one-electron states of solids. In *Solid State Physics: Advances in Research and Application*, volume 23, pages 1–181. Academix Press, New York, 1969.
217. Michael Rohlfing and Steven G. Louie, Electron-hole excitations and optical spectra from first principles, *Phys. Rev. B*, 2000, **62**(8), 4927.
218. Giovanni Onida, Lucia Reining and Angel Rubio, Electronic excitations: density-functional versus many-body Green's-function approaches, *Rev. Mod. Phys.*, 2002, **74**(2), 601.
219. Stefan Albrecht, Lucia Reining, Rodolfo Del Sole and Giovanni Onida, Ab initio calculation of excitonic effects in the optical spectra of semiconductors, *Phys. Rev. Lett.*, 1998, **80**(20), 4510.
220. Yuchen Ma and Michael Rohlfing, Optical excitation of deep defect levels in insulators within many-body perturbation theory: The f center in calcium fluoride, *Phys. Rev. B*, 2008, **77**(11), 115118.
221. Eric L. Shirley, Ab initio inclusion of electron–hole attraction: Application to x-ray absorption and resonant inelastic x-ray scattering, *Phys. Rev. Lett.*, 1998, **80**(4), 794.
222. Michael Rohlfing and Steven G. Louie, Optical excitations in conjugated polymers, *Phys. Rev. Lett.*, 1999, **82**(9), 1959.
223. Emilio Artacho, M. Rohlfing, M. Côté, P. D. Haynes, R. J. Needs and C. Molteni, Structural relaxations in electronically excited poly(paraphenylene), *Phys. Rev. Lett.*, 2004, **93**(11), 116401.
224. Michael Rohlfing and Steven G. Louie, Excitonic effects and the optical absorption spectrum of hydrogenated Si clusters, *Phys. Rev. Lett.*, 1998, **80**(15), 3320.

225. Sohrab Ismail-Beigi and Steven G. Louie, Excited-state forces within a first-principles Green's function formalism, *Phys. Rev. Lett.*, 2003, **90**(7), 076401.
226. Murilo L. Tiago and James R. Chelikowsky, Optical excitations in organic molecules, clusters, and defects studied by first-principles Green's function methods, *Phys. Rev. B*, 2006, **73**(20), 205334.
227. X. Blase and C. Attaccalite, Charge-transfer excitations in molecular donor–acceptor complexes within the many-body Bethe-Salpeter approach, *Appl. Phys. Lett.*, 2011, **99**(17), 171909.
228. X. Blase, C. Attaccalite and V. Olevano, First-principles GW calculations for fullerenes, porphyrins, phtalocyanine, and other molecules of interest for organic photovoltaic applications, *Phys. Rev. B*, 2011, **83**(11), 115103.
229. Carina Faber, Ivan Duchemin, Thierry Deutsch, Claudio Attaccalite, Valerio Olevano and Xavier Blase, Electron–phonon coupling and charge-transfer excitations in organic systems from many-body perturbation theory, *Journal of Materials Science*, 2012, **47**(21), 7472–7481.
230. Björn Baumeier, Denis Andrienko, Yuchen Ma and Michael Rohlfing, Excited states of dicyanovinyl-substituted oligothiophenes from many-body Green's functions theory, *J. Chem. Theory Comput.*, 2012, **8**(3), 997–1002.
231. Björn Baumeier, Denis Andrienko and Michael Rohlfing, Frenkel and charge-transfer excitations in donor–acceptor complexes from many-body Green's functions theory, *J. Chem. Theory. Comput.*, 2012, **8**(8), 2790–2795.
232. Ivan Duchemin and Xavier Blase, Resonant hot charge-transfer excitations in fullerene-porphyrin complexes: many-body Bethe–Salpeter study, *Phys. Rev. B*, 2013, **87**(24), 245412.
233. Denis Andrienko and Kurt Kremer, Simulations. In Krzysztofty-jaszewski, Yves Gnanou, and Ludwik Leibler, editors, *Macromolecular Engineering*, pages 1431–1469. Wiley-VCH Verlag GmbH, 2007.